Journal of Volcanology and Geothermal Research 443 (2023) 107928

Contents lists available at ScienceDirect

Journal of Volcanology and Geothermal Research

journal homepage: www.journals.elsevier.com/journal-of-volcanology-and-geothermal-research

The noble gas signature of the 2021 Tajogaite eruption (La Palma, Canary Islands)

A. Sandoval-Velasquez [a,b,*], A.L. Rizzo [c,d], F. Casetta [e], T. Ntaflos [e], A. Aiuppa [a], M. Alonso [f], E. Padrón [f,g], M.J. Pankhurst [f,g], A. Mundl-Petermeier [e], V. Zanon [h], N.M. Pérez [f,g]

[a] DiSTeM, Università di Palermo, Via Archirafi 36, 90123 Palermo, Italy
[b] Istituto Nazionale di Geofisica e Vulcanologia, Sezione di Palermo, Via Ugo La Malfa 153, 90146 Palermo, Italy
[c] Istituto Nazionale di Geofisica e Vulcanologia, Sezione di Milano, Via Alfonso Corti 12, 20133 Milano, Italy
[d] Department of Earth and Environmental Sciences, University of Milano-Bicocca, Piazza della Scienza 1, 20126 Milano, Italy
[e] Department of Lithospheric Research, University of Vienna, Josef-Holaubek-Platz 2, 1090 Vienna, Austria
[f] Instituto Volcanológico de Canarias (INVOLCAN), 38400 Puerto de la Cruz, Tenerife, Canary Islands, Spain
[g] Instituto Tecnológico y de Energías Renovables (ITER), 38600 Granadilla de Abona, Tenerife, Canary Islands, Spain
[h] Instituto de Investigação em Vulcanologia e Avaliação de Riscos, Universidade dos Açores, Rua Mãe de Deus, 9500-321 Ponta Delgada, Portugal

ARTICLE INFO

Keywords:
La Palma
2021 Tajogaite eruption
Fluid inclusions
Noble gas
Magma feeding system
Mantle source heterogeneity

ABSTRACT

Here, we characterize the temporal evolution of volatiles during the Tajogaite eruption by analyzing the elemental (He-Ar-CO_2-N_2) and isotopic (He-Ar-Ne) composition of fluid inclusions (FI) in phenocrysts (olivine+pyroxene) identified in erupted lavas. Our 2021 lava samples identify substantial temporal variations in volatile composition. We show that, during the 2021 Tajogaite eruption, the He-CO_2-N_2 concentrations in FI increased since October 15th; this increase was accompanied by increasing $^{40}Ar/^{36}Ar$ ratios (from ~300 to >500), and paralleled a major shift in bulk lava chemistry, with increasing Mg contents (Mg#, from 47 to 52 to 55–59), CaO/Al_2O_3 (from 0.65 to 0.74 to 0.75–0.90), Ni and Cr, and decreasing TiO_2, P_2O_5 and incompatible elements. The olivine core composition also became more forsteritic (from Mg# = 80–81 to Mg# = 84–86). Mineral thermobarometry and FI barometry results indicate that the eruption was sustained by magmas previously stored in at least two magma accumulation zones, at respectively ~6–12 km and 15–30 km, corroborating previous seismic and FI evidence. We therefore propose that the compositional changes seen throughout the eruption can be explained by an increased contribution - since early/mid-October - of more primitive, less-degassed magma from the deeper (mantle) reservoir. Conversely, Rc/Ra values ($^3He/^4He$ ratios corrected for atmospheric contamination) remained constant throughout the whole eruption at MORB-like values (7.38 ± 0.22 Ra, 1σ), suggesting an isotopically homogeneous magma feeding source. The Tajogaite He isotope signature is within the range of values observed for the 1677 San Antonio lavas (7.37 ± 0.17Ra, 1σ), but is more radiogenic than the $^3He/^4He$ values (>9 Rc/Ra) observed in the Caldera de Taburiente to the north. The $^3He/^4He$ ratios (6.75 ± 0.20 Ra, 1σ) measured in mantle xenoliths from the San Antonio volcano indicate a relatively radiogenic nature of the mantle beneath the Cumbre Vieja ridge. Based on these results and mixing modeling calculations, we propose that the homogeneous He isotopic signatures observed in volatiles from the Tajogaite/San Antonio lavas reflect three component mixing between a MORB-like source, a radiogenic component and small additions (6–15%) of a high $^3He/^4He$ reservoir-derived (>9Ra) fluid components. The simultaneous occurrence of high $^3He/^4He$ (>9Ra)- and MORB-like He signatures in northern and southern La Palma is interpreted to reflect small-scale heterogeneities in the local mantle, arising from spatially variable proportions of MORB, radiogenic, and high $^3He/^4He$ components.

* Corresponding author at: DiSTeM, Università di Palermo, Via Archirafi 36, 90123 Palermo, Italy.
E-mail address: andreslibardo.sandovalvelasquez@community.unipa.it (A. Sandoval-Velasquez).

https://doi.org/10.1016/j.jvolgeores.2023.107928
Received 2 May 2023; Received in revised form 22 September 2023; Accepted 6 October 2023
Available online 10 October 2023

1. Introduction

Due to its geodynamics, the characteristics of the mantle source feeding the volcanism in the Canary Islands, although having been intensively studied for decades, remains a matter of debate in the geoscience community (Troll and Carracedo, 2016; Longpré and Felpeto, 2021; Civiero et al., 2023). This volcanism have brought to the surface an enormous spectrum of volcanic rocks that testify the complexity of the local mantle source: from carbonatites, nephelinites, basanites, tephrites, tholeiitic and alkali olivine basalts associated with shield-volcanism processes to rhyodacites, rhyolites, trachytes and phonolites related to a highly explosive felsic volcanism (Schmincke, 1982; Abratis et al., 2002; Carracedo et al., 1998; Troll and Carracedo, 2016). Recent volcanism (since 1500 CE and including the 2021 Tajogaite eruption at La Palma) has been mainly characterized by effusive-like eruptions as registered in some islands such as La Palma, El Hierro, Tenerife and Lanzarote (Longpré and Felpeto, 2021). Using isotopic (noble gases, Pb, Sr, Os and Nd) evidence arising from analysis of a variety of geological materials (mantle xenoliths, crustal cumulates, lavas and surface fluids), it has been proposed that volcanism in the Canary is fed by a spatially heterogeneous mantle source, with strong, systematic east-to-west compositional gradients along the archipelago (Hoernle et al., 1991; Marcantonio et al., 1995; Hilton et al., 2000; Gurenko et al., 2006, 2009; Day and Hilton, 2011, 2021; Klügel et al., 2017; Sandoval-Velasquez et al., 2021). While the mantle beneath the western islands (La Palma, El Hierro; Fig. 1) has been shown to be dominated by high $^{3}He/^{4}He$ (>9Ra in the case of La Palma), mid-ocean ridge basalt-like (MORB) and HIMU-type (high $\mu = {}^{238}U/^{204}Pb$ ratios; Zindler and Hart, 1986) components (Hilton et al., 2000; Gurenko et al., 2006; Day et al., 2010; Day and Hilton, 2011, 2021; Sandoval-Velasquez et al., 2021), the mantle source feeding the activity of the eastern islands (Gran Canaria and Fuerteventura) has been found to be especially influenced by enriched mantle (EM) sources (Hoernle et al., 1991; Carnevale et al., 2021). In terms of noble gas systematics, the Canary Islands are one of the most enigmatic Ocean Island Basalt (OIB) localities. High $^{3}He/^{4}He$ (>9Ra) have so far been only registered in a cold spring (Dos Aguas spring; Fig. 1), and in >1.7 Ma old seamounts today surface-exposed in the Caldera de Taburiente, northern La Palma (Pérez et al., 1994; Hilton et al., 2000; Guillou et al., 2001; Gurenko et al., 2006; Day and Hilton, 2011, 2021; Padrón et al., 2015; Torres-González et al., 2020).

The recent (2021) Tajogaite eruption on La Palma Cumbre Vieja ridge (Fig. 1) represents a unique opportunity to investigate the evolution of fluid inclusions (hereafter FI) composition during a single eruption (a phenomena that is intimately related with the behavior of volatiles inside the volcano's plumbing system; e.g., Boudoire et al., 2020) and, more broadly, to deepen our understanding on the composition of mantle source beneath the western Canaries. This eruption (September 19th-December 13th, 2021), with its estimated eruptive volume of ~200 million m^3 (Bonadonna et al., 2022; Civico et al., 2022; Padrón et al., 2022), ranks as the largest historical eruption of La Palma. An initial strombolian phase was sustained by a 200 m-long fissure that formed an ash-rich plume reaching approximately 3 km in height (Carracedo et al., 2022). This explosive activity (Bonadonna et al., 2022) was accompanied by the emission of lava flows and lava fountains whose chemistry varied over time (Pankhurst et al., 2022; Carracedo et al., 2022; Day et al., 2022); in fact, early erupted lavas (before October 2021) shown more differentiated compositions (as suggested by relatively low MgO and Ni and high TiO_2) when compared with more primitive lavas emitted at latter stages (Day et al., 2022). As a result of volcanic activity, the Tajogaite cone of 200 m in height (surface 0.6 km^2) was formed, 1.180 ha were covered by lava flows (affecting banana plantations and >1000 buildings) and the island surface increased approximately 0.48 km^2 (Carracedo et al., 2022; Civico et al., 2022). Intense seismicity preceded and accompanied the eruption (Longpré, 2021; D'Auria et al., 2022; del Fresno et al., 2023).

In this work, we report on a temporally resolved record of FI volatile compositions in Tajogaite lavas. We use noble gases, in particular He, as tracers of mantle source features (Nuccio et al., 2008; Boudoire et al., 2020), and to gain insights into plumbing system processes (e.g., crystallization and degassing). FI chemistry (He-Ar-Ne-CO_2-N_2) is complemented with thermo-barometry, whole rock, mineral chemistry, and Sr-Nd-W (whole-rock) isotope results. With the aim of characterizing the spatial heterogeneity of the mantle beneath La Palma, we also compare the volatiles signature of 2021 lavas with that of: 1) basanitic lavas and entrained mantle xenoliths from the historic eruption of San Antonio volcano, and 2) a 2–4 Ma old picrite from the Caldera de Taburiente.

2. Materials and methods

The studied suite of rocks (Fig. 1) consists of: a) eight lava samples collected on the Tajogaite lava flow field, erupted between September 29th and November 9th, (Tables 1, S1 and Figs. 1 and 2); b) a lava sample from the terminal stage of the 1677 San Antonio eruption (sample LP-SA1; south of Cumbre Vieja); c) a 2–4 Ma old picrite from the Caldera de Taburiente (sample LP-BA1) collected near the picrite (sample JMDDLP03) previously analyzed by Day and Hilton (2011) from the Barranco de Angustias; and d) three mantle xenoliths (as tephra) found in the NW flank of the San Antonio volcano (samples LP-30, LP-45 and LP-54; Sandoval Velasquez et al., 2022b). The 2021 Tajogaite lava samples were collected on the developing lava flow field within one or two days from their emission. The timing of emplacement of each Tajogaite lava sample was estimated using information from INVOLCAN staff scientist in the field, and the real-time satellite data published by Copernicus (see Table S1 and Fig. 2 for coordinates and uncertainty on lava eruption time).

2.1. Whole-rock major and trace element analysis

Whole-rock major and trace element analyses were carried out on fused beads by means of a Philips PW2404 X-Ray Fluorescence (XRF) spectrometer at the Department of Lithospheric Research, University of Vienna (Austria). In order to avoid matrix interferences, the elements Na, K, Ti and P were analyzed as trace elements. Replicate analyses of geo-standard GSR-3 gave an overall procedural uncertainty better than 2% for major elements and 5% for trace elements (see Ali and Ntaflos, 2011). Rb, Sr, Y, Zr, Nb, Hf, Ta, Th, U, and REE were analyzed by means of an iCAP RQ inductively coupled plasma-mass spectrometer (ICP-MS) at the Department of Lithospheric Research, University of Vienna (Austria). For ICP-MS technique, about 0.1 g of each sample was dissolved in a 17 ml Savillex beaker using HNO3 and ARISTAR (high purified) HF, then transferred to 100 ml bottles, 5 ml and made up to final weight (100 g) with distilled 2% HNO_3. Replicate analyses of geo-standard BHVO-1 gave an overall procedural uncertainty better than 2% for all elements, except and for Th (7.5%). For the relative procedural uncertainty and accuracy of the analyses see Ali and Ntaflos (2011).

2.2. Whole-rock Sr, Nd and W isotopes

Whole-rock Sr and Nd isotopic ratios were determined using a Triton TI Thermal Ionization Mass Spectrometer (TIMS) hosted at the Department of Lithospheric Research of the University of Vienna, following the methodology described by Ferrière et al. (2010). A mean $^{87}Sr/^{86}Sr$ ratio of 0.710254 ± 0.000002 ($n = 2$) was obtained for the NBS987 (Sr) and a mean $^{143}Nd/^{144}Nd$ ratio of 0.512104 ± 0.000002 ($n = 6$) was obtained for the La Jolla (Nd) international standards during the period of investigation.

The W isotope ratios were determined at the Core Facility "Geo-Isotopes" of the Department of Lithospheric Research of the University of Vienna (DLR). Between 1 and 3 g of rock powder were digested in ~15 ml of a 1:5 mixture of concentrated HNO_3 and HF. The samples were set on a hotplate for up to one week at ~160 °C, and subsequently

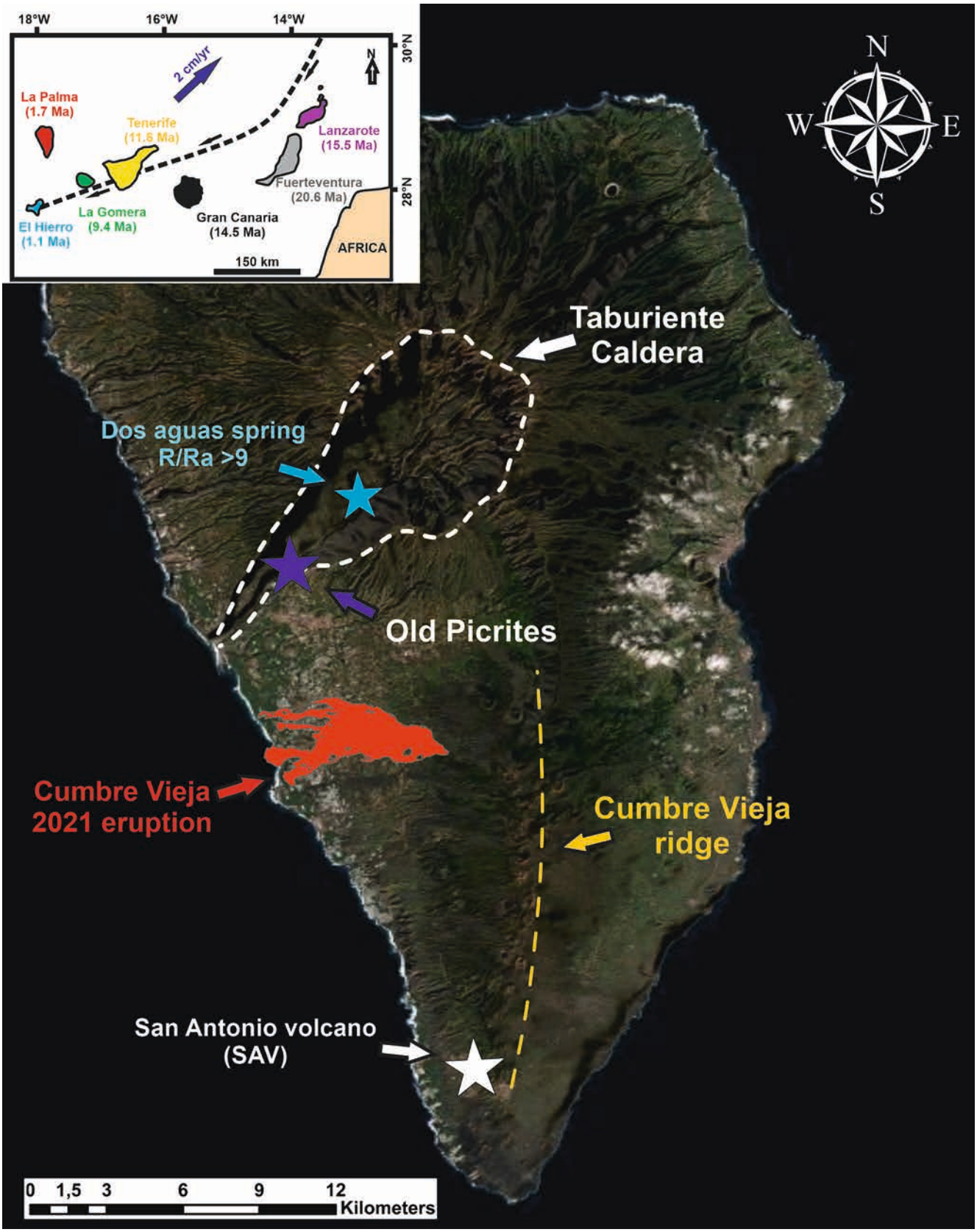

Fig. 1. Map of La Palma Island and location of the study areas. The white dotted lines represent the border of the Caldera de Taburiente and the axis of the Cumbre Vieja ridge. To the upper left of the image there is a map of the Canary archipelago, ages in million years (Ma) are the maximum ages reported in eruptive products for each Island (Anguita and Hernán, 2000; Day et al., 2010; Day and Hilton, 2021; Carracedo et al., 1998). The black dotted line indicates the likely path of the Canary hotspot (Holik et al., 1991). The lava field was designed for the period between September 27th and November 9th.

Table 1
Noble gas isotopic composition of fluid inclusions hosted in phenocrysts from the Tajogaite lavas (TV), picrites from the Caldera de Taburiente (CT) and San Antonio (SAV) lavas, as well as in crystals from San Antonio mantle xenoliths. Errors are 1σ uncertainties. [A] Replica. [B] N_2*: N_2 values corrected for atmospheric contamination during the simultaneous extraction of noble gases and CO_2. Ol = olivine; Cpx = clinopyroxene; Sp = spinel.

Sample	Locality	Lava date	Rock	Phase	^{4}He (mol/g)	^{20}Ne (mol/g)	^{40}Ar (mol/g)	CO_2 (mol/g)	N_2*B (mol/g)	Rc/Ra	(+/−)	^{40}Ar/^{36}Ar	(+/−)	^{20}Ne/^{22}Ne	(+/−)	^{21}Ne/^{22}Ne	(+/−)	^{21}Ne/^{22}Ne$_{EX}$	(+/−)
LP-BA1	CT	–	Picrite	Ol	5.81E-13	1.23E-14	6.52E-13	2.68E-11	6.78E-11	9.37	0.13	2117.9	7.9	10.36	0.05	0.0299	0.0006	0.033	0.001
LP-BA1 r[A]	CT	–	Picrite	Ol	4.79E-13	2.40E-15	1.13E-12	1.95E-11	1.94E-10	9.36	0.11	2303.0	5.8	10.38	0.16	0.0307	0.0016	0.037	0.002
LP21-AJM1	TV	29/09/2021	Basanite	Ol	7.36E-13	5.38E-15	1.57E-12	6.71E-10	1.59E-10	7.23	0.11	344.3	0.2	–	–	–	–	–	–
LP21-AJM1	TV	29/09/2021	Basanite	Cpx	1.35E-12	3.01E-14	2.03E-11	1.19E-08	1.30E-10	7.14	0.10	318.0	0.4	–	–	–	–	–	–
LP21-AJM2	TV	02/10/2021	Basanite	Ol	9.19E-13	2.05E-14	6.92E-12	1.34E-09	3.82E-10	7.55	0.09	309.6	0.2	9.98	0.04	0.0298	0.0005	0.041	0.001
LP21-AJM2	TV	02/10/2021	Basanite	Cpx	1.51E-12	5.77E-14	2.86E-11	1.71E-08	–	7.41	0.07	307.5	0.2	9.82	0.03	0.0292	0.0003	–	–
LP21-AJM3	TV	15/10/2021	Basanite	Ol	6.30E-13	1.10E-14	1.18E-12	4.78E-09	4.43E-11	7.07	0.11	366.1	0.3	9.96	0.04	0.0293	0.0007	–	–
LP21-AJM3	TV	15/10/2021	Basanite	Cpx	1.65E-12	3.18E-14	3.09E-11	2.13E-09	–	6.69	0.19	330.7	0.8	9.91	0.03	0.0293	0.0006	–	–
LP21N	TV	27/10/2027	Basanite	Ol	2.58E-12	2.65E-15	1.79E-12	1.62E-08	2.12E-09	7.20	0.10	665.5	0.8	9.96	0.10	0.0300	0.0021	–	–
LP21N	TV	27/10/2027	Basanite	Cpx	5.41E-12	3.37E-14	2.27E-11	1.41E-07	5.21E-10	7.51	0.09	372.4	0.2	9.84	0.03	0.0291	0.0004	–	–
LP21S-T1	TV	09/11/2021	Basanite	Ol	3.07E-12	4.80E-15	2.45E-12	3.04E-09	1.22E-09	7.44	0.09	881.1	1.0	–	–	–	–	–	–
LP21S-T1	TV	09/11/2021	Basanite	Cpx	3.34E-12	2.23E-14	3.01E-11	3.06E-08	–	6.03	0.15	392.6	0.6	9.82	0.03	0.0290	0.0006	–	–
LP21S-T2	TV	09/11/2021	Basanite	Ol	2.39E-12	2.28E-14	1.11E-12	3.66E-09	3.91E-10	7.74	0.11	944.4	4.0	10.28	0.05	0.0307	0.0009	0.038	0.001
LP21S-T2	TV	09/11/2021	Basanite	Cpx	3.68E-12	2.33E-14	1.61E-11	4.33E-08	–	4.66	0.29	417.3	0.2	9.91	0.05	–	–	–	–
LP21S-T3A	TV	09/11/2021	Basanite	Ol	1.16E-12	4.83E-15	1.13E-12	1.66E-09	7.85E-10	7.47	0.08	599.4	0.7	10.24	0.07	0.0305	0.0012	0.038	0.001
LP21S-T3A	TV	09/11/2021	Basanite	Cpx	3.94E-12	2.44E-14	1.39E-11	9.94E-08	2.76E-08	7.45	0.06	398.7	0.4	9.86	0.03	0.0295	0.0006	–	–
LP-SA1	SAV	–	Basanite	Ol	1.36E-12	2.16E-14	2.63E-12	2.28E-09	1.79E-10	7.31	0.08	387.4	0.2	10.26	0.05	0.0301	0.0007	0.035	0.001
LP-SA1	SAV	–	Basanite	Cpx	5.10E-12	3.16E-14	1.96E-11	1.98E-07	1.52E-08	7.36	0.06	414.9	0.6	9.85	0.04	0.0294	0.0004	–	–
LP-30	SAV	–	Sp-Harzb.	Ol	2.79E-11	7.62E-14	1.97E-11	–	1.01E-09	6.68	0.13	467.1	0.4	9.84	0.02	0.0293	0.0003	–	–
LP-45	SAV	–	Sp-Harzb	Ol	2.20E-11	4.20E-14	2.10E-16	4.77E-10	3.20E-11	6.88	0.06	632.8	0.4	9.89	0.03	0.0296	0.0003	0.046	0.001
LP-54	SAV	–	Sp-Harzb	Ol	1.78E-11	4.59E-14	2.40E-11	5.52E-10		6.83	0.12	660.3	0.4	9.87	0.02	0.0295	0.0003	0.049	0.001

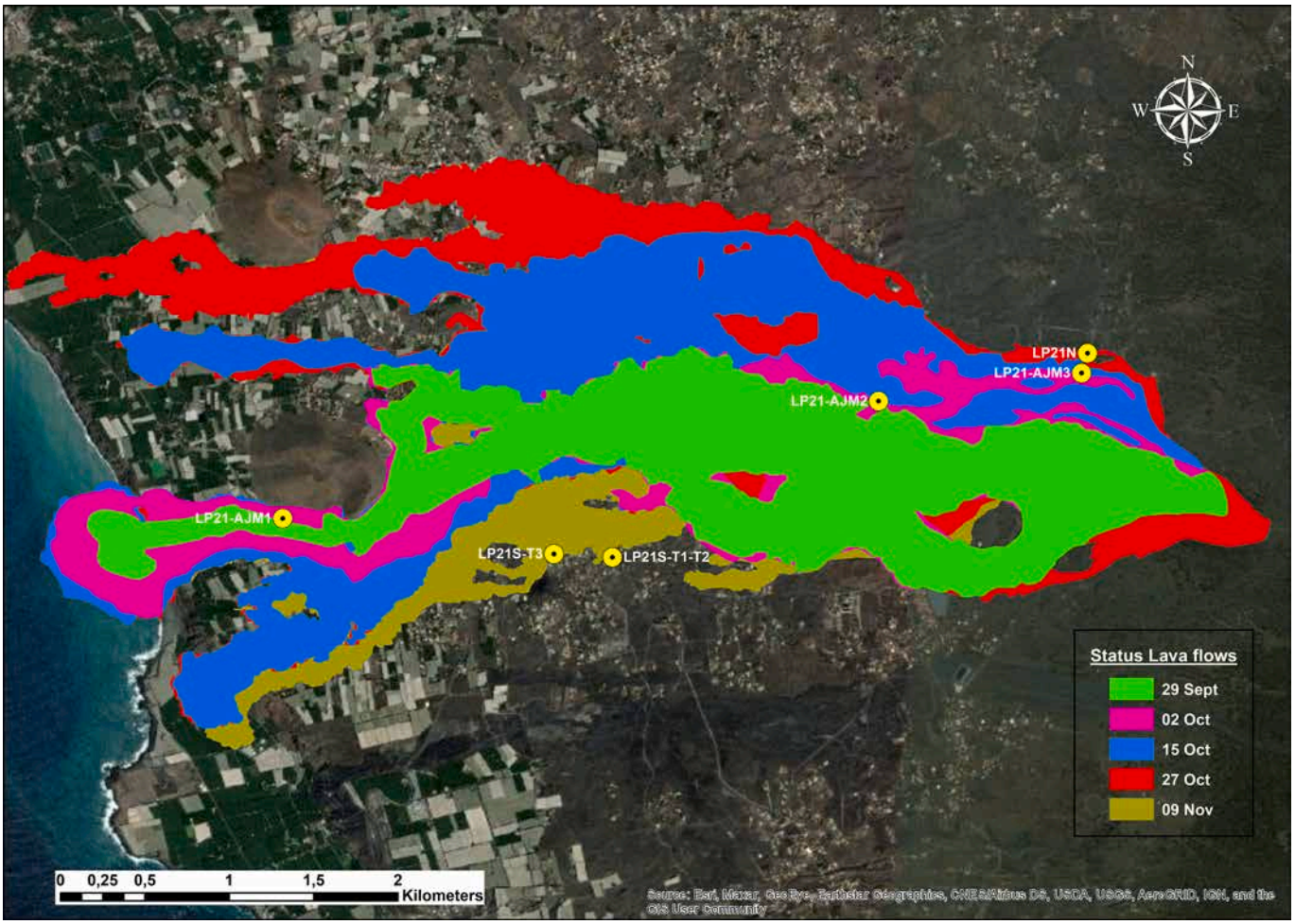

Fig. 2. Map of the lava field for the period between September 27th and November 9th. It is worth mentioning that the lava field continued growing until the end of the eruption on December 13th, 2021. The cartographic data was obtained from the COPERNICUS Emergency Management Service website.

dried down. The digested samples were then converted into chloride form by repeated addition of 8 M HCl and subsequent dried downs.

The samples where then re-dissolved in appropriate amounts of loading solution and W was purified using a three-step ion exchange chromatography method described in Peters et al. (2019). After dry-down of the final W fraction, the samples were repeatedly treated with drops of HNO_3:HCl:H_2O_2 in varying ratios to remove any organics. Approximately 1000 ng of the clean W fractions were then loaded on single *Re*-filaments and measured on a thermal ionization mass spectrometer (TIMS) following the method described in Mundl-Petermeier et al. (2022). In brief, up to 18 blocks with a total of 480 cycles consisting of two lines each, were measured with an integration time of ~34 s plus 10 s idle time per line. A peak center on mass 184 W was performed at the beginning of the measurement and after every 6th block. A 360 s baseline measurement was performed prior to the start and the rotation of the amplifiers with 10^{11} Ω resistors after every block.

The results were corrected for instrumental mass fractionation and per-integration oxide interferences according to the method described in Archer et al. (2017). To correct for oxide fractionation, $^{186}W^{16}O_2^{18}O$ and $^{187}Re^{16}O_2^{18}O$ were measured in every cycle using 10^{13} Ω resistors. The data is presented using the μ-notation, which represents the deviation of a sample's $^{182/183}$ W/^{184}W ratio to that of repeated measurements of an Alfa Aesar laboratory standard, representative of modern BSE, in parts per million. None of the samples yielded anomalous $\mu^{183}W$ (Table S2). For N-TIMS uncertainties represent the 2× standard error (2σ) of individual measurements, for MC-ICP-MS uncertainties represent the 95% confidence interval (95% CI) of individual measurements.

2.3. Petrography and mineral chemistry

The modal abundance of mineral phases and vesicles (vol%) were determined from high-resolution thin section scans by image analysis using the ImageJ software (Schneider et al., 2012). As the gray and colour scale of the constituents rarely allow to automatically threshold the thin section scan of complex natural rock samples, a manual discrimination between the chosen categories was introduced before ImageJ thresholding to minimize uncertainties. A relative error of 1–5% in modal mineral abundance can be conservatively assumed.

The major element composition of mineral phases was determined by Electron Probe Micro Analysis (EPMA), using a Cameca SXFive FE electron microprobe equipped with five wavelength-dispersive (WD) and one energy-dispersive (ED) spectrometers at the Department of Lithospheric Research, University of Vienna (Austria). Routine point analyses of olivine, oxides, clinopyroxene and amphibole were performed using the following operating conditions: 15 kV accelerating voltage, 20 nA beam current, 20 s counting time on peak position. For glasses, a 5 μm defocused beam and 10 s counting time on peak position for Na and K were used. Detection limits were: 100–250 ppm for Al, Na, Cr, Mn, Ti; 300–500 ppm for Si, Fe, Mg, Ca, Ni and K. For all analyses, natural and synthetic standards were used for calibration, and the PAP routine was applied for matrix correction (Pouchou and Pichoir, 1991).

2.4. Fluid inclusions microtherometry and Raman microspectroscopy

Fluid inclusions (FIs) microthermometry was obtained for 2 samples

of lava and tephra (Samples CAN-39 and CA-214). Samples were coarsely crushed with a jaw crusher. Crushed samples were sieved to separate crystal size populations. Olivines were then thinned up to 60–80 μm, doubly polished and observed at the microscope in search for FIs. Microthermometry was carried out on a Linkam MDSG600 heating-cooling stage, calibrated according to synthetic fluid inclusion standards of pure CO_2 and H_2O. Melting and homogenization temperatures were reproducible to ±0.1 °C with heating between 0.2 and 0.5 °C/min. Density values of the CO_2 fluid were calculated following equations 3.14 and 3.15 of (Span and Wagner, 1996). Isochores for a pure CO_2 fluid were calculated through the application of the CO_2 equation of state (Sterner and Bodnar, 1984), valid up to at least 2000 K and 10 GPa. High density values for pure CO_2 fluids in olivine were corrected for a probable pristine presence of 10% water (H_2O:CO_2 = 1:9), applying the properly correction suggested(Hansteen and Klugel, 2008). Isochores for these H_2O-CO_2 fluids were calculated in accordance with the equation provided in (Sterner and Bodnar, 1991). N_2 and CO proportions were calculated using VX diagrams (Thiery et al., 1994).

Raman microspectroscopic analyses were performed on two olivine crystals from sample CAN-214 collected at the end of the eruption that host fluid inclusions. These inclusions have melting temperatures of −56.8 to −57.3 °C, suggesting the presence of other volatile species besides CO_2 and H_2O. Fluid inclusions were analyzed using a Renishaw in Via confocal Raman micro-spectrometer, equipped with a 532 ± 0.3 nm diode laser (~180 mW output power), a CCD detector of 1040 × 256 pixels, a Rayleigh rejection edge filter, and a Leica DM 2500 M optical microscope with a motorized XYZ stage, at the Laboratoire Magmas et Volcans (France). Spectra were acquired in backscattered geometry, in both standard and high confocality modes (slit aperture of 65 and 20 μm, respectively), with a 50× microscope objective and a 2400 l/mm grating. Each acquisition consisted of two accumulations of 20 s; the laser power was set to 10% or 50% (i.e., approximately 13 and 60 mW). The spectra were recorded in extended mode from 60 to 4500 cm-1 using the WiRETM 4.4 software. Daily calibration of the spectrometer was performed using a silicon standard (520.5 cm^{-1} peak) and several Neon lines.

2.5. Noble gas isotopic compositions of fluid inclusions

The elemental and isotopic compositions of mineral-hosted fluid inclusions study were analyzed (in all samples) at the noble gas and stable isotopes laboratories of INGV, Sezione di Palermo. First, samples were crushed and sieved to hand-pick crystals of olivine (Ol), and clinopyroxene (Cpx) with diameters >0.5 mm. 13 aliquots of Ol and 8 of Cpx were selected, cleaned (using 6.5% HNO_3, deionized water and high-purity acetone), accurately weighted and subsequently loaded into an ultra-high-vacuum (UHV) crusher. Then, samples were pumped and backed for 48 h at 120 °C. With the aim of minimizing the addition of secondary helium accumulated in the crystals, the single step crushing technique was used to release gas trapped in fluid inclusions at about 200 bar and room temperature (21 °C). After crushing, CO_2 concentration is initially estimated (for each aliquot) by removing CO_2 using a "cold finger" immersed in liquid nitrogen, and then measuring the residual pressure of incondensable gases (N_2 + O_2 + noble gases). The total gas pressure (CO_2 + N_2 + O_2 + noble gases) is measured using an IONIVAC Transmitters ITR90 in a known volume of the system. Then, the gas mixture is properly purified under Zr—Al getter pumps in a UHV stainless-steel preparation line; these getters pumps have a different reactivity depending on temperature; at room temperature, the pumps mainly adsorb H_2, while at temperatures around 250–300 °C they adsorb N_2, CO_2, H_2O and other carbon compounds. After then, Ar (and Kr and Xe) was removed in a "cold finger" with active charcoal immersed in liquid nitrogen. Finally, He and Ne were adsorbed in a cold head with active charcoal cooled at 10 K and then moved at 40 and 80 K to release first He and then Ne, respectively. The isotopic abundances of He, Ne and Ar were determined using ad-hoc designed mass spectrometers: two different split-flight-tube mass spectrometers (Helix SFT-Thermo) for He and Ne, and a multi-collector mass spectrometer (Argus, GVI) for Ar. $^3He/^4He$ was corrected for contamination based on the measured $^4He/^{20}Ne$ ratio as follows:

$$Rc/Ra = \left((R_M/Ra)(He/Ne)_M - (He/Ne)_A\right)/\left((He/Ne)_M - (He/Ne)_A\right) \quad (1)$$

where subscripts A and M refer to atmospheric and measured values, respectively. Theorical $^4He/^{20}Ne$ ratio for air is 0.318 after Ozima and Podosek (2002). Analytical uncertainties (1σ) for $^3He/^4He$, $^{20}Ne/^{22}Ne$, $^{21}Ne/^{22}Ne$ and $^{40}Ar/^{36}Ar$ ratios are <6.2%, <2.0%, <5.4% and < 1.0%, respectively. The used standard was a purified aliquot of air, whose $^3He/^4He$, $^{20}Ne/^{22}Ne$ and $^{40}Ar/^{36}Ar$ reproducibility over 1 year of daily analysis was <3.5%. Typical blanks for He, Ne, and Ar were < 10^{-16}, <10^{-16} mol, and < 10^{-14} mol, respectively, being at least two orders of magnitude lower than sample signals at the mass spectrometers. Additional information is presented in Rizzo et al. (2021) and Sandoval-Velasquez et al. (2021).

3. Results

3.1. Petrography and bulk rock chemistry

The eight Tajogaite 2021 lavas (erupted between September 29th and November 9th) are moderately vesicular to massive (0–1 to <10 vol % vesicles), and are basanitic in composition (Table S2 and Supplementary Material). Phenocrysts include clinopyroxene (10–20 vol%), olivine (3–6 vol%) and Fe-Ti-oxides (<1 vol%), set in a glassy to fine-grained groundmass, made by the same mineral assemblage plus small amounts of plagioclase. Amphibole xenocrysts (<1 vol%) were found in some samples of the September 29th flow (AJM-1; Figs. S1-S3) that have slightly more evolved composition (MgO contents of 7.3–7.8 wt%). The subsequent flows (erupted during October and November 2021) have a more primitive character, with MgO of 8.2–9.4 wt%, higher abundance of clinopyroxene and olivine, and occasionally show the presence of small, cm-sized fragments of mantle peridotites (Figs. S4 to S9). Our data shows an increase in MgO with the progress of the eruption between September and November accompanied by an increase in Ni and Cr, and a decrease in TiO_2, P_2O_5 and in all incompatible elements (Fig. 3). This coincide with the geochemical variations observed by Day et al. (2022) who reported low MgO, Ni and Cr contents at the beginning of the eruption which would progressively increase until day 20; subsequently the contents would stabilize until day 70 when a slightly decrease, particularly in MgO, was observed until the end of the eruption (Day et al., 2022).

Regarding the pre-historical picrite, this crops out in the SW of Caldera de Taburiente (Fig. 1) and is part of the submarine lavas and breccia sequences constituting the basal part of the Pliocenic seamount stage of La Palma (Carracedo et al., 2001). It is constituted by large olivine crystals (35–40 vol%), partially replaced by serpentine, and minor amounts of small clinopyroxene (<1 vol%) and Fe—Ti oxides (<1 vol%) immersed in a microcrystalline groundmass. It has 29.6 wt% MgO, 1.4 wt% TiO_2 and 975 ppm Ni. On the other hand, the 1677 San Antonio lava flow (see Fig. 1) is massive (1–3 vol% vesicles), and contains olivine (5–6 vol%), clinopyroxene (15–20 vol%) and Fe—Ti oxides (<1 vol%), set in a glassy to fine-grained groundmass, made by the same mineral assemblage plus plagioclase (Fig. S10). It has basanitic composition, comparable to that of the most primitive products erupted during the 2021 event (8.5 wt% MgO, 4.0 wt% TiO_2, 105 ppm Ni). Finally, the selected mantle xenoliths collected from the San Antonio cone include three spinel-harzburgite (LP-30, LP-45, LP-54), with protogranular to slightly porphyroclastic textures. In the harzburgites, orthopyroxene shows reaction textures, being locally replaced by secondary clinopyroxene, olivine and glass (Fig. S11).

The PM-normalized incompatible element pattern of all lava samples exhibits the classic OIB-like signature (Fig. S12) previously reported for

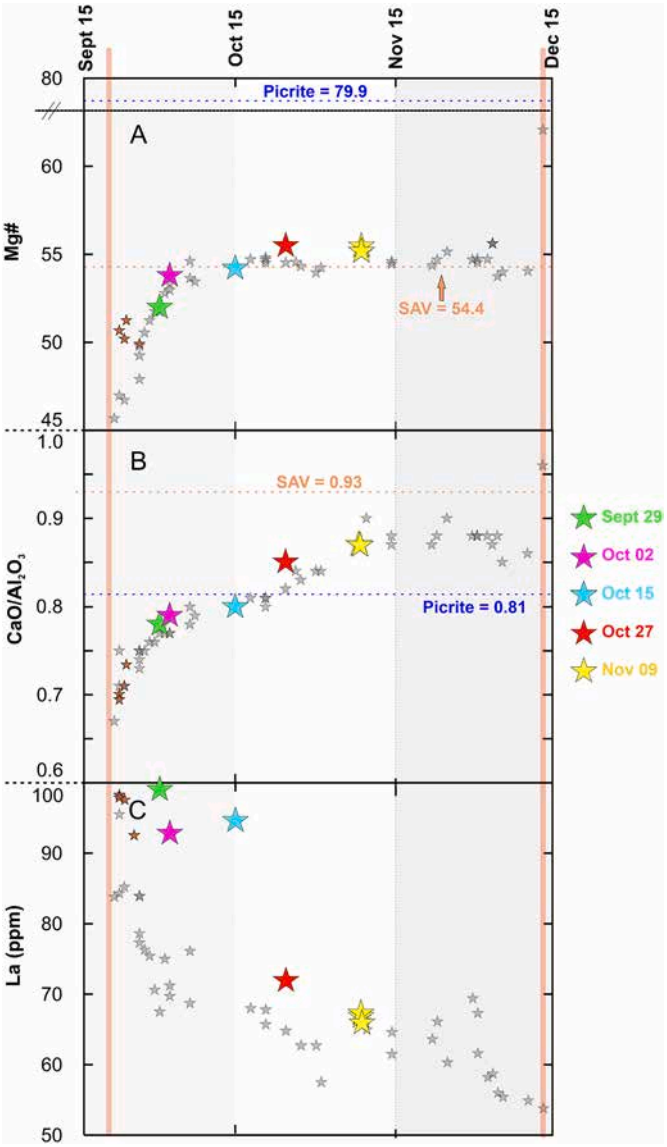

Fig. 3. Temporal variation of bulk Mg#, CaO/Al_2O_3 and La. Small gray and brown stars represent data from the literature: Day et al. (2022) and Pankhurst et al. (2022), respectively. Orange and dark blue dotted lines represent the averages for the San Antonio lava (SAV) and the picrite, respectively. Red lines represent the beginning and the end of the eruption. (For interpretation of the references to colour in this figure legend, the reader is referred to the web version of this article.)

La Palma historical and pre-historical lavas (Carracedo et al., 2001; Gurenko et al., 2006; Day et al., 2010; Klügel et al., 2017). Sr—Nd and W isotopic results are reported in Table S2 and Figs. S13-S14.

3.2. Mineral chemistry and thermobarometry of the 2021 Tajogaite lavas

In September 2021 Tajogaite samples, olivine phenocrysts have euhedral to skeletal shape, and usually host numerous inclusions of Fe—Ti oxides. They are sometimes slightly reverse zoned, with $Fo_{80–81}$ euhedral cores surrounded by $Fo_{82–83}$ rims, and sometimes normal zoned, with Fo_{83} cores surrounded by Fo_{79} rims (Table S3). In samples LP-21-ST1, T2, T3 (erupted on November 9th), euhedral to skeletal shaped olivine grains vary from slightly reverse zoned to occasionally Fo-rich cores ($Fo_{84–86}$) surrounded by $Fo_{79–80}$ rims. In all samples, clinopyroxene is mildly to complexly zoned, with either rounded resorbed or euhedral Al-Ti-diopside cores (Mg# from 60 to 78) sometimes Na-rich surrounded by Mg-Cr-enriched domains (Mg# 79–83) and then by Na-poor, Al-Ti-diopsidic rims. Frequently, clinopyroxene + Fe—Ti oxide coronas surround olivine phenocrysts. Amphibole in sample AJM1 has Fe-kaersutitic composition, with Mg# 64–72, ~6.0 wt% TiO_2, 2.5–2.6 wt% Na_2O and 1.0–1.2 wt% K_2O.

Olivine-melt thermometry suggest that olivine crystallization in the more mafic basanitic melt began at 1217–1237 °C, while olivine crystallization in the slightly evolved basanitic melt took place at 1156–1178 °C (Table S4). Clinopyroxene-melt thermobarometry indicates that the most Mg-rich diopsidic clinopyroxene crystallized in equilibrium with a basanitic melt at T = 1172–1175 °C and P of 390–470 MPa, while the Al-Ti-diopsidic domains yield equilibrium with a slightly evolved basanitic-tephritic melt at T of 1110–1157 °C, at P varying between 36 and 643 MPa. The most Fe-rich clinopyroxene domains attain equilibrium with a phonolitic melt composition and record colder crystallization conditions (T = 969–1023 °C) at comparable P (290–473 MPa). Single-mineral thermobarometry applied to amphibole indicate that the crystallization of this phase took place at similar T and P (1035–1062 °C, 486–531 MPa). Hygrometric models suggest that the H_2O content during amphibole crystallization in a likely evolved phonolitic melt was comprised between 3.6 and 4.8 wt%.

3.3. Microthermometry and Raman microspectroscopy

Fluid inclusions hosted in olivines from samples CAN-39 and CAN-214 collected on october 5th and november 6th 2021, respectively, were analyzed for thermobarometric determinations (Table S5). The inclusions mostly formed during event of late stage fracturing of the host crystal and show re-equilibration textures as commonly observed in other oceanic volcanoes (Zanon et al., 2020). Upon heating, frozen inclusions melted at temperatures (Tm) that vary between −56.6 and −57.1 °C. These temperatures are compatible with a fluid composition made of pure CO_2 ± micromoles of other volatile species. Raman microspectroscopic analysis was performed on two olivine crystals from sample CAN-214 (collected on November 6, 2021), revealing the presence of N_2 at 0.03 to 0.04 mol% levels (estimated using VX diagrams; Thiery et al., 1994). Homogenization temperatures to the liquid phase (ThL) ranged between 1.1 and 31.0 °C in sample CAN-39, and between −9.9 and 31.0 °C in sample CAN-214. The corresponding densities range from 963 to 492 kg/m^3 (CAN39) and from 1027 to 496 kg/m^3 (CAN-214). Ten inclusions from CAN-214 sample homogenized to vapor phase (ThV) at 30.8 °C, corresponding to a density of 416 kg/m^3. The calculated re-equilibration pressures form polymodal distributions, with a common population at 624–825 MPa in both samples. The basanite from October 5 (sample CAN-39) shows a second pressure population at 348–452 MPa. Single-value barometric modes are present in both samples from 314 to 171 MPa. Pressures are converted into depths according to the La Palma crustal model of (Zanon et al., 2020), and correspond to ~22.5–29 km depth for the common population, ~13.0–16.5 km depth for the population present in the October 5 sample. The scattered modes correspond to depths of ~11.5 to 6.1 km (Fig. S15). All depths are calculated from the sea level.

3.4. Noble gas and CO_2 compositions

CO_2 is the most abundant volatile species in all samples, followed by N_2* (N_2 corrected for atmospheric contamination) and noble gases (Table 1). The picrite is the most depleted in ^{4}He (<6×10^{-13} mol/g) and CO_2 (<3×10^{-13} mol/g). The Tajogaite lavas exhibit a systemic temporal increase in He-CO_2-N_2 abundances for the period between September and early November (Fig. 4A-B-C): samples erupted after October 15th exhibit higher contents (^{4}He > 2.00×10^{-8} mol/g; CO_2 (in cpx) > 3.00×10^{-8} mol/g; N_2* > 3.90×10^{-10} mol/g) relative to pre-October 15th samples (LP-21-AJM1, AJM2 and AJM3). An increase in $^{40}Ar/^{36}Ar$ ratios, particularly in olivine, is also observed (from <300 to >500) (Fig. 4D). For comparison, the San Antonio lavas have $^{40}Ar/^{36}Ar$

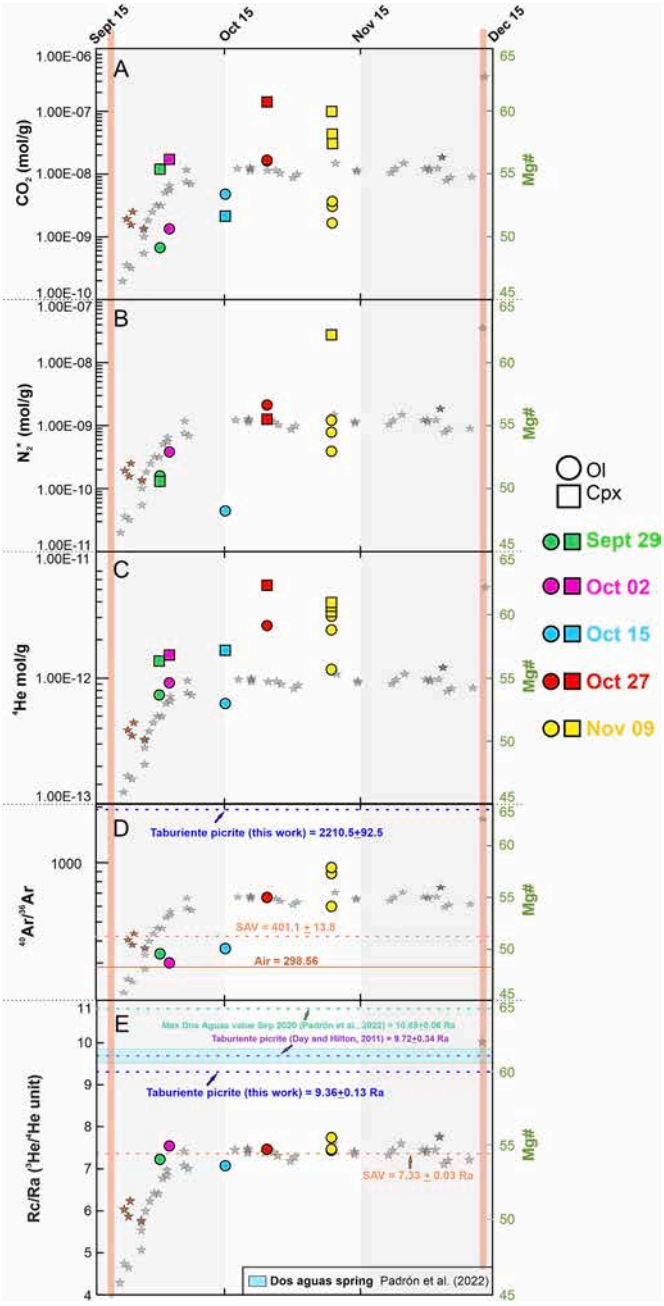

Fig. 4. Temporal variation of He, CO_2 and N_2 concentrations and $^{40}Ar/^{36}Ar$ and Rc/Ra ($^3He/^4He$ ratio corrected for atmospheric contamination) ratios between September 29th and November 9th. Gray and brown stars in figures A-E represents the variability of bulk Mg# after Day et al. (2022) and Pankhurst et al. (2022), respectively. Orange and dark blue dotted lines represent the averages for the San Antonio lava (SAV) and the picrite here studied, respectively. The light blue represents the variability of $^3He/^4He$ in the Dos Aguas spring during the eruption. Red lines indicate the beginning and the end of the eruption. (For interpretation of the references to colour in this figure legend, the reader is referred to the web version of this article.)

ratios of 401 ± 13.8 (1σ). Rc/Ra values are relatively constant throughout the entire Tajogaite eruption (Fig. 4E), and overlap with the San Antonio lavas range. The average Rc/Ra value for the Tajogaite eruption is 7.38 ± 0.22 Ra (1σ) similar to the value observed in the San Antonio lava (7.33 ± 0.33, 1σ). In contrast, the picrite from Taburiente exhibits higher $^{40}Ar/^{36}Ar$ (2210.5 ± 92.5, 1σ) and Rc/Ra (of 9.36 ± 0.13, 1σ), the latter comparable to that previously reported by Day and Hilton (2011) (Fig. 4D, E). Olivine from mantle xenoliths show the highest He concentrations (on average 2.38 × 10^{-11} ± 3.29 × 10^{-12} mol/g) and the lowest Rc/Ra values, with an average of 6.75 ± 0.20 Ra (1σ), more radiogenic than MORB (8 ± 1Ra; Graham, 2002). The $^{21}Ne/^{22}Ne_{EX}$ ratios for Tajogaite/San Antonio lavas are calculated by extrapolating the measured $^{21}Ne/^{22}Ne$ ratios to Neon-B ($^{20}Ne/^{22}Ne$ = 12.5), after Graham (2002) and Halldórsson et al. (2014); only samples with $^{20}Ne/^{22}Ne$ distinguishable from air are selected. The estimated $^{21}Ne/^{22}Ne_{EX}$ vary in a narrow range for the Tajogaite lavas, between 0.35 and 0.44, with the Taburiente picrite showing the lowest ratios (0.33 to 0.37) and mantle xenoliths exhibiting the highest (0.46 to 0.49).

4. Discussion

Monitoring noble gases at active volcanoes contributes to understanding the dynamics of magmatic plumbing systems, and the mechanisms that trigger volcanic eruptions (Burnard, 2013). However, previous studies have primarily focused on noble gas ($^3He/^4He$ especially) compositional changes in superficial emissions, and their link to volcano behavior (Nuccio et al., 2008; Padrón et al., 2013; Sano et al., 2015; Rizzo et al., 2015; Boudoire et al., 2020; Álvarez-Valero et al., 2022). On the other hand, less attention has been paid to resolving the noble gas temporal variability in FI in lavas erupted within a single, specific eruption (e.g., Nuccio et al., 2008; Boudoire et al., 2020).

The 2021 Tajogaite eruption at La Palma, in view of the rapid eruption monitoring response (Carracedo et al., 2022; Pankhurst et al., 2022; D'Auria et al., 2022; del Fresno et al., 2023), the accessibility of sampling spots and the primitive nature of the OIB-type lavas, offered an unprecedented chance to investigate noble gas variations in FI. In the following sections, we show that noble gas contents and isotopic ratios (e.g., $^{40}Ar/^{36}Ar$) in Tajogaite lavas registered substantial temporal changes throughout the eruption. This information, combined with whole-rock chemistry, mineral chemistry, FI barometry, and He-Sr-Nd-W isotopic data, contributes to refining our understanding of the eruption feeding system, and of the mantle source composition beneath La Palma Island.

4.1. Temporal changes in the chemistry of the Tajogaite lavas

Our whole-rock analyses confirm the substantial temporal shifts in major/trace element lava composition throughout the Tajogaite eruption, already documented by other authors (Pankhurst et al., 2022; Day et al., 2022) (Fig. 3). While lavas from the opening phase of the 2021 Tajogaite eruption (September 21st-29th) are chemically more evolved and often entrain fragments of amphibole-bearing gabbroic assemblages, lava flows erupted in October to November exhibit more primitive signatures, as indicated by their higher bulk Mg# and CaO/Al_2O_3 ratios (Fig. 3A-B) and lower La (and other incompatible elements) concentrations (Fig. 3C). It is worth mentioning that Mg# tend to decrease at the end of the eruption when erupting materials become more evolved (Day et al., 2022). In addition, the composition of the cores of olivine phenocrysts shifts from $Fo_{79–82}$ in September products up to $Fo_{86–89}$ in the products emitted after October 15th (Table S3). Indeed, in these later flows (starting with sample LP-21 N), olivine modal abundances increase, amphibole is absent, and mantle microxenoliths appear (Ntaflos et al., 2022), confirming the increasing primitivity of the products (Figs. S4-S9).

A novel aspect of our results is that the volatile contents in FIs also experience similar, previously unidentified, temporal changes during the eruption. The He, Ar, N_2 and CO_2 concentrations in FI vary little from September 29 to October 15, as the bulk-rock and mineral chemistry (Fig. 4A-C). Since October 27, however, CO_2 N_2 and He concentrations all increase, reaching concentrations of up to 1.41 × 10^{-7}, 2.76 × 10^{-8} and 3.94 × 10^{-12} mol/g, respectively (Fig. 4A-C), i.e., the highest in our dataset.

The noble gas isotopic compositions of olivine-hosted FI are illustrated in Fig. 4D-E. Several studies (Hilton et al., 1995, 2000; Day and

Hilton, 2011) have proved that He diffusivity is higher in clinopyroxene than in olivine; therefore, clinopyroxene is more prone to incorporate crustal helium (at magmatic temperatures) when magma migrates to the surface, being less robust than olivine for tracking the deep mantle-derived features. In our dataset, $^{40}Ar/^{36}$ Ar and $^{3}He/^{4}He$ measured in clinopyroxene-hosted FI are considerably lower than in cogenetic olivines, particularly in samples LP-21-AJM3, LP-21-ST1 and LP-ST2 (Table 1). We ascribe these lower He—Ar isotopic ratios to the effect of secondary processes, such as atmospheric contamination and/or diffusive loss of helium (Hilton et al., 1993, 1995; Lages et al., 2021). As these processes can potentially modify the original primitive FI composition (Hilton et al., 1993, 1995), clinopyroxene-hosted FI will not be considered in the following discussion.

The measured $^{40}Ar/^{36}$ Ar ratios in FI reveal systematic temporal fluctuations during the 2021 Tajogaite eruption (Fig. 4D). It is worth mentioning that the $^{40}Ar/^{36}Ar$ ratio is a sensible indicator of contamination by atmosphere-derived fluids (Graham, 2002; Burnard, 2013). In early samples (LP-21-AJM1, AJM2 and AJM3), a relatively homogenous signature around 300 (close to the atmospheric ratio of 298.6; Lee et al., 2006) is observed, while in lavas erupted after October 15th $^{40}Ar/^{36}Ar$ ratios are 2–3 times the initial values registered in September. We stress that our $^{40}Ar/^{36}Ar$ ratios are all well below the MORB-range (44,000; Moreira et al., 1998), implying that all FI underwent some level of contamination by atmospheric fluids (congruent with the magmatic nature of our samples). Yet, the abrupt $^{40}Ar/^{36}$ Ar isotopic ratio increase in the earlier-erupted Tajogaite samples suggests a higher contribution of deeper mantle-derived fluids (and/or the extent of atmospheric contamination decreased) since late-October.

In contrast to Ar isotopes, He isotopes do not exhibit any systematic variation during the eruption, with $^{3}He/^{4}He$ values remaining constant at MORB-like values of 7–7.5 Ra, similar to those reported in lavas collected from other localities of the Cumbre Vieja ridge (Fig. 4E) (Hilton et al., 2000; Gurenko et al., 2006; Day and Hilton, 2011). This invariant isotope signature indicates that Tajogaite olivines record an isotopically homogeneous (at least for He) magmatic source during the entire eruption. Notably, the MORB-like He signature of the Tajogaite lavas is in stark contrast with the high $^{3}He/^{4}He$ mantle component observed in the Dos Aguas Spring (Caldera de Taburiente) in the same time period (Padrón et al., 2022). The nearly invariant He—Nd, He—Sr, and He—W isotope couples also support an isotopically homogeneous source (Figs. S13, S14).

4.2. The feeding system of the Tajogaite eruption

The noble gas results can be better understood if interpreted in view of copious emerging evidence for a dual magma reservoir system feeding to the Tajogaite eruption (Day et al., 2022; D'Auria et al., 2022; Dayton et al., 2023; del Fresno et al., 2023). Seismicity records (Fig. 5) indicate a bimodal distribution of hypocenter depths during the eruption, with a deep cluster at ~20 to 30 km and a shallow cluster at ~6 to 12 km (D'Auria et al., 2022; Dayton et al., 2023). A similar bimodality – but shifted deeper in the magmatic system at 33–38 km and 9–13 km - was observed by del Fresno et al. (2023) (possibly because these authors used a simplified 1D velocity model). Notably, the pre-eruptive (11–19 September) and initial *syn*-eruptive (19 September-early October) seismicity was limited to shallow depths, indicating that the initial phase of the eruption was sustained by dyke intrusion of magma accumulated since 2017 at ~10 km depth, near the local Moho (Figs. 5-6A) (Torres-González et al., 2020; Padrón et al., 2022; D'Auria et al., 2022; Dayton et al., 2023; del Fresno et al., 2023). This ~10 km magma storage zone, at the base of the ocean crust, has been active during all historical eruptions of Cumbre Vieja (Klügel et al., 2005, 2015). The pressure estimates derived from clinopyroxene-melt thermobarometry confirm that clinopyroxene crystals from all samples record crystallization in a

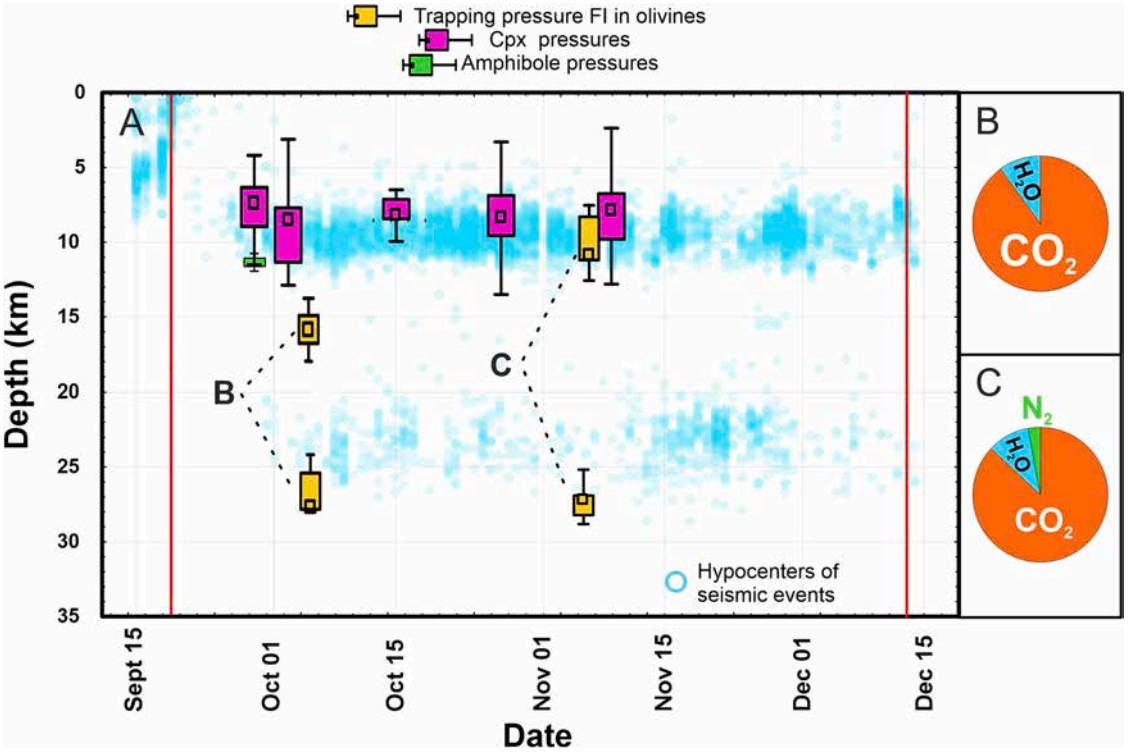

Fig. 5. A) Syn-eruptive seismicity beneath the Tajogaite volcano for the period between September 15th and December 15th 2021; data is from the INVOLCAN. Red lines indicate the beginning and the end of the eruption. Boxplots were designed based on the mineral and FI data of Tables S4 and S5. B) Composition of olivine-hosted FI in lavas erupted on October 5th where the main recognized volatiles phases are CO_2 and H_2O through microthermometry and Raman microspectroscopy analysis (Table S5). This contrasts with the C) composition of olivine-hosted FI in lavas erupted on November 6th, where N_2 is also identified. (For interpretation of the references to colour in this figure legend, the reader is referred to the web version of this article.)

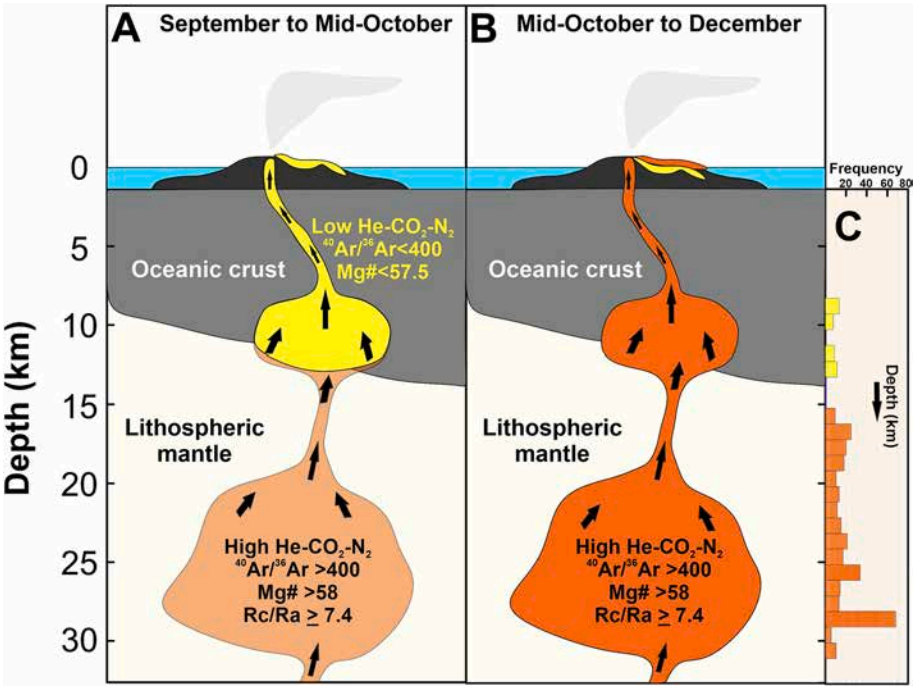

Fig. 6. Envisioned model for the plumbing system of the 2021 Tajogaite volcano based on the mineral and volatile compositions. Further information is provided in Section 4.2. The thickness of the oceanic crust was taken from Martinez-Arevalo et al. (2013) and D'Auria et al. (2022). C) The histogram shows the distribution of the FI barometric data reported in Table S5 and data from Dayton et al. (2023).

ponding zone located between 4 and 12 km (Fig. 5). Thermobarometry models based on amphibole-melt pairs, characterized by narrower uncertainties, indicate that the xenocryst cargo in the early erupted samples equilibrated in a magma storage zone located between 11 and 12 km (Fig. 5). On the other hand, seismic data record the activation of a deep (~20 to 30 km) reservoir only since early October 2021, indicating that deeper rising magma was increasingly participating into feeding the eruption (D'Auria et al., 2022; Dayton et al., 2023). This deep magma storage zone is not recorded by crystallization pressures derived by clinopyroxene-melt barometry but is well tracked by FI entrapment pressures obtained via calibrated Raman spectroscopy in olivine-hosted FI (Dayton et al., 2023). Indeed, our microthermometry (heating-cooling stage) results show that the entrapment pressures of olivine-hosted FI coherently capture both the shallow and deep magma storage/stagnation zones (Fig. 5). These pressure estimates from olivines, based on the analysis of two different samples collected within a month of each other (early October and early November; Table S5), identify two regions for FI trapping (or re-equilibration) that perfectly match the two syn-eruptive seismicity clusters (Fig. 5). This is also consistent with the progressive replenishment of the volcanic conduit by the arrival of mafic magma where olivine was in equilibrium.

A model in which early lavas (September), derived from a previously accumulated shallow magma at ~10 km (Fig. 6A), were later (since mid-October) progressively replaced by more primitive deeper rising melts (Fig. 6B) (D'Auria et al., 2022; Day et al., 2022; Pankhurst et al., 2022; del Fresno et al., 2023), is also consistent with the observed variations in the chemistry of CO_2 and noble gas inside FI, whose content progressively increase with the proceeding of the eruption (Fig. 4). Carbon dioxide, N_2 and He are all characterized by low solubility in silicate melts at mantle depths (Papale et al., 2022). For example, CO_2 solubility in La Palma basanitic melts at ~10 km depth is predicted by solubility models to be only 0.25 to 0.6 wt% (Jiménez-Mejías et al., 2022). Therefore, if the Tajogaite parental (undegassed) melt contained several wt% CO_2, as typical for alkaline ocean islands melts (Aiuppa et al., 2021), then this means that the majority (>90%) of CO_2 must have been segregated into a separated fluid phase during magma storage in the shallower (~6 to 12 km) reservoir. In this scenario, the CO_2-depleted September 2021 products could bear witness of a long term storage in the Cumbre Vieja feeding system, during which CO_2 was lost into a separated fluid phase. Likewise, this long-term storage could have caused the loss of N_2, whose concentration is also low in September products (Fig. 4B). Indeed, N_2 is a volatile species with very low solubility in silicate melts (Keppler et al., 2022), and is enriched in the fluid phase during degassing at higher pressure than CO_2 and He (Libourel et al., 2003; Bernadou et al., 2021). A shallow (~6 to 12 km) stored magma is thus expected to have already exsolved most of its N_2 (and Ar) to gas bubbles, justifying the N_2-depleted nature of FI from the initial phase of the eruption (Fig. 6A). It is important to remark that N_2 was not detected by our microthermometric FI analysis on the October 5 lavas, while it became increasingly detectable (at 0.03 to 0.04 mol% level) in the later products of the eruption (in the November 6, 2021 sample). The progressive increase of N_2, He and CO_2 in the erupted olivines (Fig. 4), coupled to an increase in olivine Fo content is entirely consistent with a scenario in which the arrival of N_2-rich, less-degassed melts, rising from the deeper source (15–30 km) progressively replenished the feeding system of the Tajogaite eruption (Fig. 6B-C).

A dual magma storage zone feeding the Tajogaite eruption can also explain the evolution of $^{40}Ar/^{36}Ar$ during the eruption (Fig. 4D). As Ar is especially prone to atmospheric contamination, a variety of mechanisms could have contributed to lower $^{40}Ar/^{36}Ar$ ratios of the early-erupted lavas. First, it is well possible that stored magmas interacted, during ponding, with Jurassic oceanic crust materials that, having suffered extensive seafloor alteration, likely contains an atmospheric Ar component (Parley and Craig, 1994); in fact, Day et al. (2022) reported low Os contents, more radiogenic $^{187}Os/^{188}Os$ and high $^{187}Re/^{188}Os$ in early lavas (day 1–20 lavas) which likely points to assimilation of sedimentary or volcanic materials. Secondly, seismic tomography studies (D'Auria et al., 2022) indicate that the Tajogaite dyke, during its upward migration from the ~10 km magma storage zone, rose at the western boundary between consolidated oceanic crust and a shallow (<3 km) hydrothermal alteration body, made of highly fractured, unconsolidated hydrothermally altered volcanic materials (Di Paolo et al.,

2020). This fractured hydrothermal body might have easily acted as an additional source of atmospheric Ar during shallow magma emplacement. We then argue that, as the magma path to the surface matures with the progress of the eruption, the interaction with atmospheric components was progressively reduced, leading to the observed increase in the $^{40}Ar/^{36}Ar$ ratio up to 945 (Fig. 4D). The FI hosted in mineral phases in mantle xenoliths from San Antonio have $^{40}Ar/^{36}Ar$ ratios (467–587) comparable to those measured in FI of the later erupted Tajogaite lavas and those previously reported in the literature for pyroxenites (Tazacorte, Fuente Santa and San Antonio volcanoes), a picrite and ankaramites (Caldera de Taburiente and Garafia volcano) (Day and Hilton, 2011; Day, 2022), implying that (i) the mantle source underneath Cumbre Vieja is likely the repository of an atmospheric Ar component, (ii) San Antonio mantle xenoliths entrapped secondary FI degassed at about underplating depths, and (iii) the later lavas are more prone to reflect the signature of the underlying mantle, confirming the deep (mantle) supply to the later stages of the eruption (Fig. 6B).

The above proposed model for magma storage zone model can be also reconciled with the restricted variation of $^{3}He/^{4}He$ ratios seen during the eruption (Fig. 4E). The 50 years-long dormancy of Cumbre Vieja before the Tajogaite eruption suggests that, at least until October 2017, the ~10 km deep magma ponding zone consisted of small residual melt lenses remnant of previous eruptions (Fig. 6A). Long residence times of melt in the crust cause magma aging driven by differentiation processes, degassing and continuous production of ^{4}He derived from radioactive decay of U—Th (Torgersen and Jenkins, 1982; Hilton et al., 1993; Burnard, 2013); thus, the residual melts in the plumbing system (or magmatic material kept in "cold storage" at low temperature that could be subsequently reinvigorated; e.g., Jackson et al., 2018) were likely characterized by low $^{3}He/^{4}He$ (<7Ra). However, between October 2017 and August 2021, the feeding system of the Tajogaite eruption was increasingly injected by magma rising from the upper mantle to the base of the oceanic crust (Torres-González et al., 2020; D'Auria et al., 2022; Padrón et al., 2022; del Fresno et al., 2023). We argue that this pre-eruptive recharge of mantle-sourced melts may have easily reset any previously inherited He signature for the old resident magma, and therefore homogenized the $^{3}He/^{4}He$ of the entire shallow plumbing system, determining the temporally invariant MORB-like signature seen in all Tajogaite samples. It is important to observe that He is less prone than Ar to atmospheric contamination, being thus nearly unaffected by an eventual pre- to *syn*-eruptive interaction with hydrothermalized material as proposed to explain the $^{40}Ar/^{36}Ar$ variations.

4.3. The mantle source beneath Cumbre Vieja ridge

Radiogenic and stable isotopic systematics (He-Sr-Nd-Pb-Os-O) have contributed to identifying a complex and chemically heterogeneous mantle underneath the western Canary Islands. At La Palma, in particular, three distinct mantle components, mixing in various proportions, have been proposed in the literature to explain the He isotope composition of surface fluids, lavas and cumulitic materials (Day and Hilton, 2011): (i) a high $^{3}He/^{4}He$ endmember(> 9 Rc/Ra) [3]; (ii) a MORB-like component (Rc/Ra of ~8), and (iii) a radiogenic (Rc/Ra of 4–6) recycled oceanic lithosphere (ROL) end-member, that is especially needed to explain the He—O variability of La Palma volcanics. Gurenko et al. (2006, 2009), based on He-Sr-Nd-Pb evidence, further elaborated on the three-mantle component model, suggesting that a high $^{3}He/^{4}He$ component with HIMU affinity mixes within a dominantly depleted shallow (lithospheric) mantle source (MORB-type component), and that the radiogenic component may correspond to an enriched mantle (EM) component entrained in the plume (and similar to that seen in the eastern islands; Fig. S13; Table S2; Hoernle et al., 1991; Gurenko et al., 2006; Day et al., 2010; Klügel et al., 2017), and matches closely the composition of the HIMU component of Gurenko et al., 2009 (Fig. S13B and C).

Our observations here, and especially those taken on mantle xenoliths in San Antonio lavas, offer for the first time an opportunity to directly evaluate the helium isotopic signature of the lithospheric mantle beneath the Cumbre Vieja ridge. The studied mantle xenoliths are spinel harzburgites (Sandoval Velasquez et al., 2022c), and thus representative of a local lithospheric mantle. These xenoliths have higher ^{4}He, lower $^{3}He/^{4}He$ (6.79 ± 0.19 Rc/Ra, 1σ; $n = 3$), and similar $^{40}Ar/^{36}Ar$, relative to the Tajogaite/San Antonio lavas (Table 1). This contrasts with the information obtained from mantle rocks in the neighboring island of El Hierro, where mantle xenoliths have relatively higher $^{40}Ar/^{36}Ar$ ratios (>1000) and MORB-like $^{3}He/^{4}He$ signature (Sandoval-Velasquez et al., 2021). Low $^{3}He/^{4}He$ and high $^{40}Ar/^{36}Ar$ ratios have been also verified in an ankaramite sample from Taburiente and harzburgites from Lanzarote (Day and Hilton, 2011; Day, 2022). Our observations, therefore, provide direct evidence for the previously identified (Gurenko et al., 2006, 2009; Day and Hilton, 2011) radiogenic He component in the La Palma mantle source.

The nature/origin of this radiogenic component underneath La Palma is puzzling. In the Canary Islands, low $^{3}He/^{4}He$ ratios in mantle-derived rocks have been previously observed only in the eastern islands (for example in lavas from Gran Canaria and Sp-harzburgites from Lanzarote), and associated with the presence of an Enriched Mantle (EM) radiogenic component, possibly derived from the African Sub Continental Lithospheric mantle (Vance et al., 1989; Hoernle et al., 1995; Day and Hilton, 2021; Sandoval Velasquez et al., 2022b) and/or simply represent a "refractory mantle" endmember (Day, 2022). However, no evidence for the involvement of such components has been found in primitive lavas from the western islands (Day et al., 2010, 2022). Therefore, we consider more likely that the relatively low radiogenic (6.75 ± 0.20 Rc/Ra, 1σ) signature of the San Antonio xenoliths reflects a recycled oceanic (crustal/lithospheric) component in the local mantle (the ROC/ROL components of Day and Hilton, 2011). Helium-Sr-Nd-Pb analysis in the same mantle xenolith suite is required to better characterize the origin of this radiogenic component.

If the local lithospheric mantle underneath Cumbre Vieja is then relatively radiogenic, the MORB-like He signature of the Tajogaite lavas require some further explanation. As He-Sr-Nd isotopes are relatively invariant at La Palma (Fig. S13), we rely on Ne isotopes as more sensible tracers of fluid provenance. In a $^{4}He/^{3}He$ vs $^{21}Ne/^{22}Ne_{EX}$ plot (Fig. 7), the Cumbre Vieja (Tajogaite/San Antonio) lavas fall in an intermediate position between the Taburiente picrites, plotting close to the high $^{3}He/^{4}He$ component, and the San Antonio xenoliths, which represent the radiogenic term (with Rc/Ra < 7). We therefore interpret the intermediate isotopic ratios of Tajogaite/San Antonio lavas as resulting from mixing, in various proportions, of the three distinct isotopic reservoirs/components described above (i.e., high $^{3}He/^{4}He$ (>9Ra), MORB, and a recycled radiogenic component; Day and Hilton, 2011). To test this hypothesis, we modelled two different mixing scenarios. In scenario 1 (Fig. 7A), we model three component mixing between (a) a high $^{3}He/^{4}He$ component with Rc/Ra = 11 (corresponding to the maximum $^{3}He/^{4}He$ observed in the Dos Aguas Spring; Padrón et al., 2022) and $^{21}Ne/^{22}Ne_{EX} = 0.034$ (Hilton et al., 2000; Graham, 2002; Day and Hilton, 2011; Halldórsson et al., 2014); (b) a MORB-like component, with Rc/Ra = 8 ± 1 Ra and $^{21}Ne/^{22}Ne_{EX} = 0.06$ (Graham, 2002); and (c) a radiogenic endmember with Rc/Ra of 6.79 and $^{21}Ne/^{22}Ne_{EX} = 0.047$ (the averages of our mantle xenoliths). Scenario 2 (Fig. 7B) differs from the previous only for an higher Rc/Ra (of 15) assumed for the high $^{3}He/^{4}He$ endmember (in order to match the maximum $^{3}He/^{4}He$ reported for the central Atlantic region; Madureira et al., 2005). In both cases, the Tajogaite/San Antonio lavas fall close to the local mantle- high $^{3}He/^{4}He$ component mixing trend; their compositions are therefore consistent with the addition of small contributions of the high $^{3}He/^{4}He$ domain (10–15% and 6–8% in scenario 1 and 2, respectively) to a heterogeneous, relatively radiogenic lithospheric mantle. We caution that our measured Ne isotope ratios ($^{20}Ne/^{22}Ne$ and $^{21}Ne/^{22}Ne$) have mean ± 1 σ values (we adopt here the 1 σ uncertainty level used in Hopp et al., 2004, 2007; Lupton et al., 2012; Halldórsson et al., 2014) exceeding the

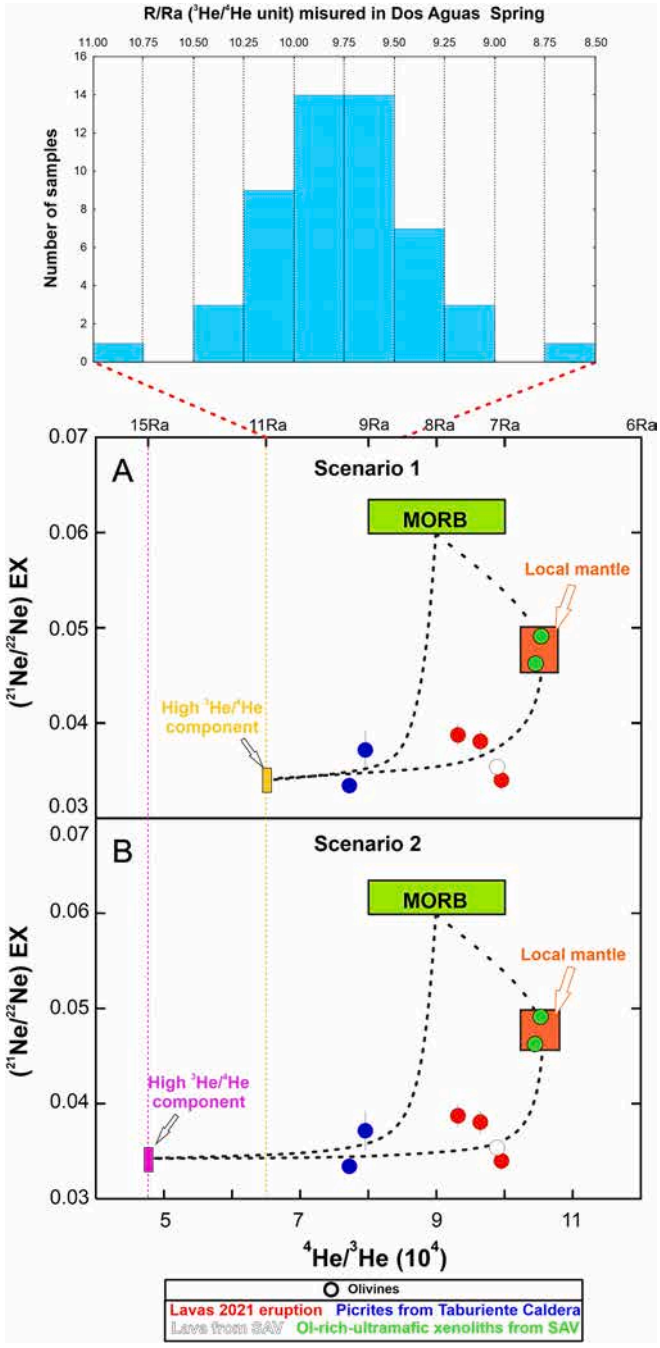

Fig. 7. $^{4}He/^{3}He$ vs $^{21}Ne/^{22}Ne_{EX}$. $^{21}Ne/^{22}Ne_{EX}$ values were calculated by extrapolating the measured $^{21}Ne/^{22}Ne$ ratios to Neon-B ($^{20}Ne/^{22}Ne = 12.5$) after Graham (2002) and Halldórsson et al. (2014). Only samples with $^{20}Ne/^{22}Ne$ distinguishable from air were selected at the 1σ level. Dotted lines are binary mixing trends between three endmembers: A) Plume endmember at 11Ra and $^{21}Ne/^{22}Ne_{EX} = 0.034 \pm 0.001$, a MORB-like reservoir at 8.0 Ra and $^{21}Ne/^{22}Ne_{EX} = 0.06 \pm 0.001$ (Graham, 2002) and a radiogenic reservoir at 6.79 Ra and $^{21}Ne/^{22}Ne_{EX} = 0.047 \pm 0.001$. B) Same as A except for the assumed plume endmember at 15Ra and $^{21}Ne/^{22}Ne_{EX} = 0.034 \pm 0.001$, please see Subsection 4.3 for more details. As comparison, the histogram at the top of the panels A and B shows the distribution of R/Ra values measured in the Dos Aguas Spring (values from Pérez et al., 1994; Hilton et al., 2000; Padrón et al., 2015; Torres-González et al., 2020; Day and Hilton, 2021; Padrón et al., 2022).

atmospheric ratios, but are within the atmospheric range if mean ± 2 σ values (as in Day, 2022) are considered instead. This means that our calculated $^{21}Ne/^{22}Ne_{EX}$ values (Fig. 7) have meaning only at 1 σ level, and should therefore treated with caution. We argue however that, in addition to Ne isotopes, the heterogeneous, multi-component nature of the La Palma mantle source is corroborated by stable (O) and radiogenic (Pb, Os) isotopes (Hilton et al., 2000; Gurenko et al., 2006; Day and Hilton, 2011, 2021; Day, 2022), and supported by the systematic differences in $^{3}He/^{4}He$ signatures shown here and in previous work (Fig. 7).

In summary, the MORB-like signature of the Tajogaite/San Antonio lavas may not represent a mantle endmember itself. Rather, it could merely reflect the result of mixing between Canarian high $^{3}He/^{4}He$ component and more radiogenic mantle reservoirs. This interpretation is consistent with previous models (e.g., Hilton et al., 2000; Gurenko et al., 2006; Day and Hilton, 2011) where both high $^{3}He/^{4}He$ and MORB components dominate the noble gas signature of the mantle source feeding the Cumbre Vieja volcanism (Fig. 8). We caution that our Ne isotope results are within the 2σ.

4.4. Implications for the spatial $^{3}He/^{4}He$ heterogeneity of La Palma volcanism

Compared to other ocean islands such as Hawaii or Iceland (where $^{3}He/^{4}He$ ratios can reach values >30Ra), the Canary Islands are characterized by relatively modest lower mantle contributions. As shown above, the Tajogaite lavas have $^{3}He/^{4}He$ ratios within the MORB range. In combination with their tungsten isotopic compositions ($\mu^{182}W = 1.3 \pm 2.4$), our samples fall in the so-referred Ambient Mantle field of Mundl-Petermeier et al. (2020) in terms of He—W isotopes (Fig. S14), implicating relatively marginal contribution from the deep mantle (as exemplified by the Core Mantle Equilibrated Reservoir, CMER; Mundl-Petermeier et al., 2020). Therefore, upper mantle materials are largely involved in the genesis of both the Tajogaite lavas and the 2–4 Ma old Taburiente picrites.

In addition to being relatively low in primordial ^{3}He, the Canary archipelago is characterized by large isotopic heterogeneity at both regional and local (within a single island) scales. At La Palma, in particular, a systematic $^{3}He/^{4}He$ difference between the northern and southern sectors exists (Hilton et al., 2000; Day and Hilton, 2011; Padrón et al., 2015, 2022; Torres-González et al., 2020). Our samples confirm this chemical diversity. The 1677 San Antonio eruption in the south emitted several lava flows of basanitic-tephritic composition that created a new coastal platform. Their noble gas compositions (Rc/Ra =7.33 ± 0.03 and $^{40}Ar/^{36}Ar = 401.14 \pm 13.79$) are very similar to those of the Tajogaite 2021 lavas (Fig. 4) and other Cumbre Vieja products (Hilton et al., 2000; Gurenko et al., 2006; Day and Hilton, 2011; Torres-González et al., 2020). In contrast, the Taburiente picrite sample cropping out to the north of La Palma has a more primitive composition, as indicated by higher $^{40}Ar/^{36}Ar$ and $^{3}He/^{4}He$ ratios (Fig. 4). This relatively high $^{3}He/^{4}He$ ratio (Rc/Ra = 9.36 ± 0.01 (1σ); Figs. 4 and 7) matches the compositions of the picrite previously analyzed by Day and Hilton (2011) and the dissolved gases in the Dos Aguas cold spring (Pérez et al., 1994; Gurenko et al., 2006; Day and Hilton, 2011, 2021; Padrón et al., 2022), and confirms a high $^{3}He/^{4}He$ reservoir for northern La Palma. It is worth noting that, in northern La Palma, both high (Rc/Ra > 9) and more radiogenic (Rc/Ra of 6.3–7 Ra) FI compositions coexist (Hilton et al., 2000; Day and Hilton, 2011), implicating an isotopically heterogeneous mantle source.

The coexistence of high $^{3}He/^{4}He$ (Taburiente) and MORB-like (Cumbre Vieja) signatures in a single ocean island makes La Palma unique not only in the context of the Canary archipelago, but also in the context of OIB volcanism. Similar spatial $^{3}He/^{4}He$ ratio variations have only been observed at Heard Island in the southern Indian Ocean (Hilton et al., 1995) and at Pico and Terceira Island, in the Azores archipelago (Moreira et al., 1999; Madureira et al., 2005). At Heard Island, the two

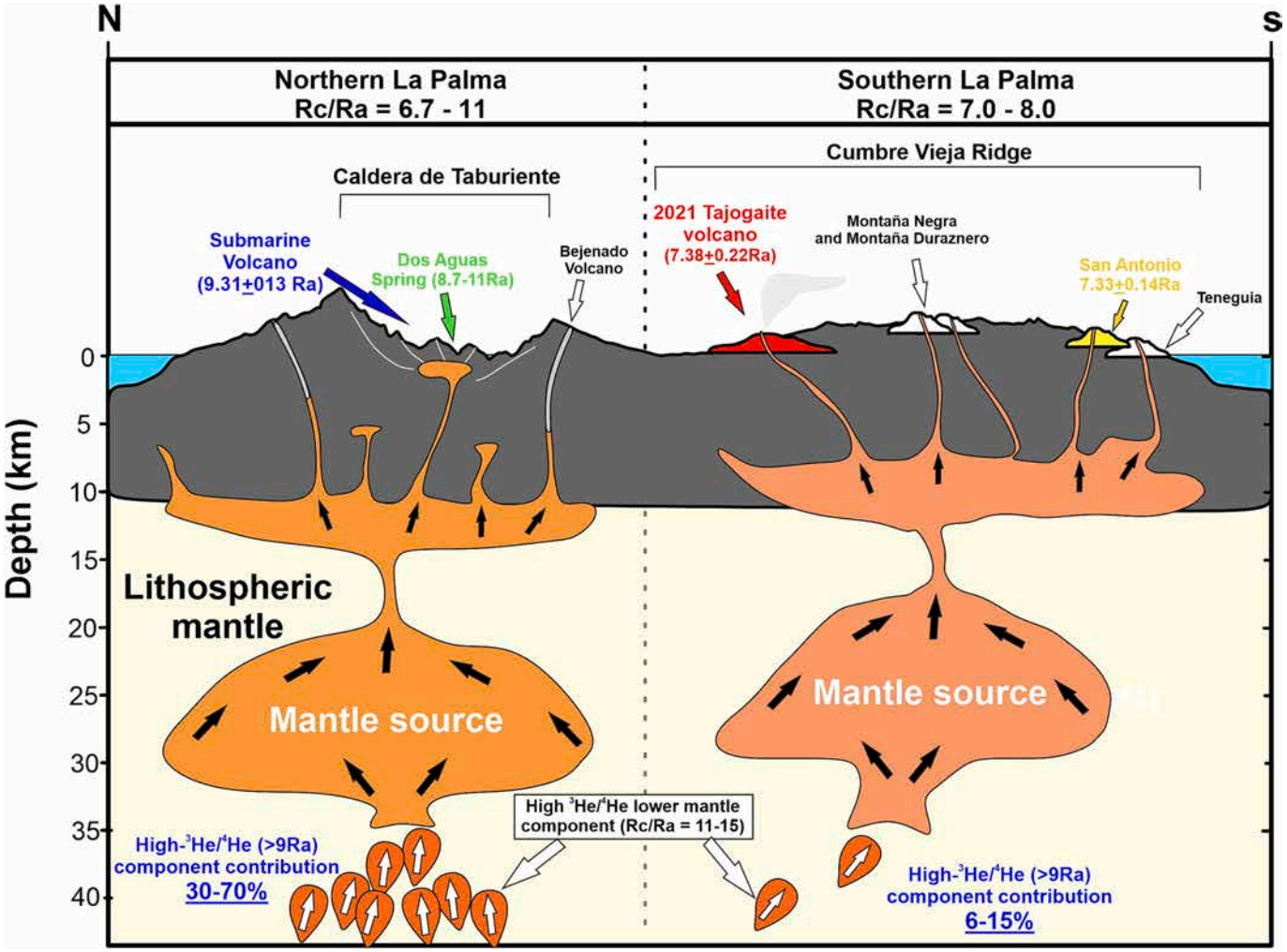

Fig. 8. Cross-section (N-S) for La Palma island showing the interpreted plumbing system for northern and southern La Palma. $^{3}He/^{4}He$ values from the submarine, Tajogaite and San Antonio volcanoes are presented in Table 1. The $^{3}He/^{4}He$ ranges for the Dos Aguas spring as for northern and southern La Palma were determined using the data from this work and from the literature (Pérez et al., 1994; Hilton et al., 2000; Gurenko et al., 2006; Day and Hilton, 2011, 2021; Padrón et al., 2015, 2022; Torres-González et al., 2020). The main magmatic reservoirs were designed using the mineral and FI data presented in Tables S4 and S5 and from the literature. The thickness of the oceanic crust was taken from Martinez-Arevalo et al. (2013) and D'Auria et al. (2022). Contributions of the high $^{3}He/^{4}He$ component were estimated using the mixing curve between the radiogenic domain (local mantle) and the high $^{3}He/^{4}He$ component shown in Fig. 7 which are the result of mass-balance and isotopic mass balance equations.

coeval Laurens Peninsula and Big Ben volcanic centers exhibit very diverse $^{3}He/^{4}He$ signatures, i.e., 16.2–18.3 Ra vs. 5–8.4 Ra, respectively (Hilton et al., 1995). This discrepancy has been ascribed to the contribution of a lower mantle component beneath the former, and to shallow addition of radiogenic He caused by crustal contamination beneath the latter (Hilton et al., 1995; Graham, 2002). On the other hand, the $^{3}He/^{4}He$ variability in historic lavas at Pico and Terceira, from MORB-like values of 7–9 Ra to relative primitive ratios of up to 15 Ra has been attributed to compositional heterogeneities in the mantle source (Moreira et al., 1999; Madureira et al., 2005).

At La Palma, crustal contamination has been discarded as the cause for the reported low $^{3}He/^{4}He$ in lava phenocrysts (Pérez et al., 1994; Hilton et al., 2000; Gurenko et al., 2006; Padrón et al., 2015, 2022). The Tajogaite/San Antonio lavas are fresh and gas-rich mafic samples, and the single step crushing technique we used prevented from the addition of secondary helium (see Section 2). In view of our mixing models above (Fig. 7), we thus propose that the isotopic variability observed at La Palma is linked to small-scale heterogeneities in the local mantle (Fig. 8). We propose that the Taburiente picrites record a larger contribution of the high $^{3}He/^{4}He$ reservoir (from ~60–70% to ~30–40%; Fig. 7A-B) than the Tajogaite/San Antonio lavas (6–15%) (Fig. 8). These small scale heterogeneities would have remained relatively invariant at least during the last 0.15 Ma, since the formation of the Cumbre Vieja ridge (Guillou et al., 1998; Troll and Carracedo, 2016).

5. Conclusions

We have characterized the noble gases elemental and isotopic composition of FI in phenocrysts from the 2021 Tajogaite eruption at La Palma. Our results can be summarized as follows:

1) He-CO_2-N_2 contents and $^{40}Ar/^{36}Ar$ ratios of mineral-hosted FI increased during the 2021 Tajogaite eruption, particularly after October 15th. This paralleled increases in bulk rock Mg# and CaO/Al_2O_3, the increase in the Ni, and Fo content of olivine cores. These observations are consistent with a major change in the plumbing system dynamics, associated with the arrival of a more primitive less-degassed basanitic magma from the mantle into a more mature and degassed ponding zone located at ca. 10 km of depth;
2) Mineral-melt thermobarometry and FI barometry confirm the existence of two main magma accumulation regions located at 6–12 km and 15–30 km. We envision a model in which early lavas

(September-early October) derived from an older and degassed magma accumulated in the shallow reservoir, that was subsequently fed with more primitive basanitic melt by mid-October;

3) The constant MORB-like $^{3}He/^{4}He$ ratio observed in both early and late Tajogaite lavas are ascribed to pre-eruptive recharge of mantle-sourced melts since October 2017. Injections of magmas with MORB-like He would have reset and re-homogenized the $^{3}He/^{4}He$ of the shallow plumbing system (at least in the ~15–30 km to ~6–12 km depth range), explaining the temporally invariant He signature of all Tajogaite samples;
4) Peridotite xenoliths from San Antonio exhibit $^{3}He/^{4}He$ values below 7Ra, suggesting the presence of a radiogenic lithospheric mantle component beneath Cumbre Vieja. Mixing models suggest that the signatures of Tajogaite/San Antonio lavas come from a radiogenic/MORB reservoir whose isotopic composition derived from <15% addition of high $^{3}He/^{4}He$-like fluids (>9Ra);
5) Olivines of the Taburiente picrite trap FI with 9.31 ± 0.13Ra, 1σ. These are comparable to values in the Dos Aguas spring and confirm a more pronounced high-$^{3}He/^{4}He$ component contribution (up to 30–70%) in the genesis of some magmatic products at La Palma. We propose that the isotopic dichotomy between magmatic products from the same island is caused by a variability in the mixing proportions of three mantle components (radiogenic, MORB and high-$^{3}He/^{4}He$).

CRediT authorship contribution statement

A. Sandoval-Velasquez: Conceptualization, Investigation, Formal analysis, Data curation, Writing – original draft, Visualization. **A.L. Rizzo:** Conceptualization, Methodology, Formal analysis, Writing – review & editing, Supervision. **F. Casetta:** Data curation, Formal analysis, Investigation, Writing – review & editing. **T. Ntaflos:** Writing – review & editing. **A. Aiuppa:** Conceptualization, Methodology, Formal analysis, Writing – review & editing, Supervision. **M. Alonso:** Resources. **E. Padrón:** Resources, Writing – review & editing. **M.J. Pankhurst:** Writing – review & editing. **A. Mundl-Petermeier:** Data curation, Formal analysis, Writing – review & editing. **V. Zanon:** Resources, Data curation, Formal analysis, Writing – review & editing. **N.M. Pérez:** Resources, Writing – review & editing.

Declaration of Competing Interest

The authors declare that they have no known competing financial interests or personal relationships that could have appeared to influence the work reported in this paper.

Data availability

Data will be made available on request.

Acknowledgements

This research was funded by the Italian Minister (PRIN2017LMN-LAW and 2022HA8XCS), by the Deep Carbon Observatory, by the Project MAGAT (Ref. CIRCNA/OCT/2016/2019), funded by the Fundação para a Ciência e Tecnologia (FCT), Portugal, by the RETURN Extended Partnership funded by the European Union Next-GenerationEU (National Recovery and Resilience Plan – NRRP, Mission 4, Component 2, Investment 1.3 – D.D. 1243 2/8/2022, PE0000005), by the National Biodiversity Future Center (National Recovery and Resilience Plan – NRRP, Mission 4, Component 2, Investment 1.4, CN00000033) and by the projects VOLRISKMAC II (MAC2/3.5b/328), co-financed by the EC Cooperation Transnational Program MAC 2014-2020, and "Cumbre Vieja Emergencia", financed by the Spanish Ministry of Science and Innovation. AM-P acknowledges funding from FWF grant V659-N29. The Authors thank Dr. Joao Lages and Marcello Bitetto for helping with sample collection of the early lavas. We thank Ilka Wünsche for thin sections preparation and Franz Kiraly for support during EPMA analyses. We are grateful to Monika Horschinegg for Sr—Nd isotope analyses. We also thank Mariano Tantillo and Mariagrazia Misseri for helping in sample preparation and during the isotope analysis of noble gases performed in the noble gas laboratory of INGV-Palermo. We are also grateful to Federica Schiavi Laboratoire Magma et Volcans, Université Clermont Auvergne, France for providing Raman measurements.

Finally, we thank Prof. James Day and Dr. Samantha Tramontano for their valuable comments which improved our manuscript.

Appendix A. Supplementary data

Supplementary data to this article can be found online at https://doi.org/10.1016/j.jvolgeores.2023.107928.

References

Abratis, M., Schmincke, H.-U., Hansteen, T., 2002. Composition and evolution of submarine volcanic rocks from the central and western Canary Islands. Int. J. Earth Sci. 91, 562–582. https://doi.org/10.1007/s00531-002-0286-7.

Aiuppa, A., Bitetto, M., Delle Donne, D., La Monica, F.P., Tamburello, G., Coppola, D., Della Schiava, M., Innocenti, L., Lacanna, G., Laiolo, M., Massimetti, F., Pistolesi, M., Silengo, M.C., Ripepe, M., 2021. Volcanic CO_2 tracks the incubation period of basaltic paroxysms. Sci. Adv. 7, eabh0191. https://doi.org/10.1126/sciadv.abh0191.

Ali, S., Ntaflos, T., 2011. Alkali basalts from Burgenland, Austria: petrological constraints on the origin of the westernmost magmatism in the Carpathian–Pannonian Region. Lithos 121, 176–188. https://doi.org/10.1016/j.lithos.2010.11.001.

Álvarez-Valero, A.M., Sumino, H., Caracausi, A., Sánchez, A.P., Burgess, R., Geyer, A., Borrajo, J., Rodríguez, J.A.L., Albert, H., Aulinas, M., Núñez-Guerrero, E., 2022. Noble gas isotopes reveal degassing-derived eruptions at Deception Island (Antarctica): implications for the current high levels of volcanic activity. Sci. Rep. 12, 19557. https://doi.org/10.1038/s41598-022-23991-3.

Anguita, F., Hernán, F., 2000. The Canary Islands origin: a unifying model. J. Volcanol. Geotherm. Res. 103, 1–26. https://doi.org/10.1016/S0377-0273(00)00195-5.

Archer, G.J., Mundl, A., Walker, R.J., Worsham, E.A., Bermingham, K.R., 2017. High-precision analysis of 182 W/ 184 W and 183 W/ 184 W by negative thermal ionization mass spectrometry: per-integration oxide corrections using measured 18 O/ 16 O. Int. J. Mass Spectrom. 414, 80–86. https://doi.org/10.1016/j.ijms.2017.01.002.

Bernadou, F., Gaillard, F., Füri, E., Marrocchi, Y., Slodczyk, A., 2021. Nitrogen solubility in basaltic silicate melt - implications for degassing processes. Chem. Geol. 573, 120192 https://doi.org/10.1016/j.chemgeo.2021.120192.

Bonadonna, C., Pistolesi, M., Biass, S., Voloschina, M., Romero, J., Coppola, D., Folch, A., D'Auria, L., Martin-Lorenzo, A., Dominguez, L., Pastore, C., Reyes Hardy, M., Rodríguez, F., 2022. Physical characterization of long-lasting hybrid eruptions: the 2021 Tajogaite eruption of Cumbre Vieja (La Palma, Canary Islands). J. Geophys. Res. Solid Earth 127. https://doi.org/10.1029/2022JB025302.

Boudoire, G., Rizzo, A.L., Arienzo, I., Di Muro, A., 2020. Paroxysmal eruptions tracked by variations of helium isotopes: inferences from Piton de la Fournaise (La Réunion island). Sci. Rep. 10, 9809. https://doi.org/10.1038/s41598-020-66260-x.

Burnard, P. (Ed.), 2013. The Noble Gases as Geochemical Tracers, Advances in Isotope Geochemistry. Springer, Heidelberg; New York.

Carnevale, G., Caracausi, A., Correale, A., Italiano, L., Rotolo, S., 2021. An overview of the geochemical characteristics of oceanic carbonatites: new insights from Fuerteventura carbonatites (Canary Islands). Minerals 11, 203. https://doi.org/10.3390/min11020203.

Carracedo, J.C., Day, S., Guillou, H., Rodríguez Badiola, E., Canas, J.A., Pérez Torrado, F. J., 1998. Hotspot volcanism close to a passive continental margin: the Canary Islands. Geol. Mag. 135, 591–604. https://doi.org/10.1017/S0016756898001447.

Carracedo, J.C., Badiola, E.R., Guillou, H., 2001. Geology and volcanology of la Palma and El Hierro, Western Canaries. Estud. Geol. 57, 175–273.

Carracedo, J.C., Troll, V.R., Day, J.M.D., Geiger, H., Aulinas, M., Soler, V., Deegan, F.M., Perez-Torrado, F.J., Gisbert, G., Gazel, E., Rodriguez-Gonzalez, A., Albert, H., 2022. The 2021 eruption of the Cumbre Vieja volcanic ridge on La Palma, Canary Islands. Geol. Today 38, 94–107. https://doi.org/10.1111/gto.12388.

Civico, R., Ricci, T., Scarlato, P., Taddeucci, J., Andronico, D., Del Bello, E., D'Auria, L., Hernández, P.A., Pérez, N.M., 2022. High-resolution digital surface model of the 2021 eruption deposit of Cumbre Vieja volcano, La Palma, Spain. Sci. Data 9, 435. https://doi.org/10.1038/s41597-022-01551-8.

Civiero, C., Carvalho, J., Silveira, G., 2023. Mantle structure beneath the Macaronesian volcanic islands (Cape Verde, Canaries, Madeira and Azores): a review and future directions. Front. Earth Sci. 11, 1126274. https://doi.org/10.3389/feart.2023.1126274.

D'Auria, L., Koulakov, I., Prudencio, J., Cabrera-Pérez, I., Ibáñez, J.M., Barrancos, J., García-Hernández, R., Martínez van Dorth, D., Padilla, G.D., Przeor, M., Ortega, V., Hernández, P., Peréz, N.M., 2022. Rapid magma ascent beneath La Palma revealed

by seismic tomography. Sci. Rep. 12, 17654. https://doi.org/10.1038/s41598-022-21818-9.
Day, J.M.D., 2022. Noble gas isotope systematics in the Canary Islands and implications for refractory mantle components. Geochim. Cosmochim. Acta 331, 35–47. https://doi.org/10.1016/j.gca.2022.06.002.
Day, J.M.D., Hilton, D.R., 2011. Origin of 3He/4He ratios in HIMU-type basalts constrained from Canary Island lavas. Earth Planet. Sci. Lett. 305, 226–234. https://doi.org/10.1016/j.epsl.2011.03.006.
Day, J.M.D., Hilton, D.R., 2021. Heterogeneous mantle-derived helium isotopes in the CanaryIslands and other ocean islands. Geology. https://doi.org/10.1130/G47676.1.
Day, J.M.D., Pearson, D.G., Macpherson, C.G., Lowry, D., Carracedo, J.C., 2010. Evidence for distinct proportions of subducted oceanic crust and lithosphere in HIMU-type mantle beneath El Hierro and La Palma, Canary Islands. Geochim. Cosmochim. Acta 74, 6565–6589. https://doi.org/10.1016/j.gca.2010.08.021.
Day, J.M.D., Troll, V.R., Aulinas, M., Deegan, F.M., Geiger, H., Carracedo, J.C., Pinto, G. G., Perez-Torrado, F.J., 2022. Mantle source characteristics and magmatic processes during the 2021 La Palma eruption. Earth Planet. Sci. Lett. 597, 117793 https://doi.org/10.1016/j.epsl.2022.117793.
Dayton, K., Gazel, E., Wieser, P., Troll, V.R., Carracedo, J.C., La Madrid, H., Roman, D.C., Ward, J., Aulinas, M., Geiger, H., Deegan, F.M., Gisbert, G., Perez-Torrado, F.J., 2023. Deep magma storage during the 2021 La Palma eruption. Sci. Adv. 9, eade7641. https://doi.org/10.1126/sciadv.ade7641.
del Fresno, C., Cesca, S., Klügel, A., Domínguez Cerdeña, I., Díaz-Suárez, E.A., Dahm, T., García-Cañada, L., Meletlidis, S., Milkereit, C., Valenzuela-Malebrán, C., López-Díaz, R., López, C., 2023. Magmatic plumbing and dynamic evolution of the 2021 La Palma eruption. Nat. Commun. 14, 358. https://doi.org/10.1038/s41467-023-35953-y.
Di Paolo, F., Ledo, J., Ślęzak, K., Martínez van Dorth, D., Cabrera-Pérez, I., Pérez, N.M., 2020. La Palma island (Spain) geothermal system revealed by 3D magnetotelluric data inversion. Sci. Rep. 10, 18181. https://doi.org/10.1038/s41598-020-75001-z.
Ferrière, L., Koeberl, C., Thöni, M., Liang, C., 2010. Single crystal U–Pb zircon age and Sr–Nd isotopic composition of impactites from the Bosumtwi impact structure, Ghana: comparison with country rocks and Ivory Coast tektites. Chem. Geol. 275, 254–261. https://doi.org/10.1016/j.chemgeo.2010.05.016.
Graham, D.W., 2002. Noble gas isotope geochemistry of mid-ocean ridge and ocean island basalts: characterization of mantle source reservoirs. Rev. Mineral. Geochem. 47, 247–317. https://doi.org/10.2138/rmg.2002.47.8.
Guillou, H., Carracedo, J.C., Day, S.J., 1998. Dating of the Upper Pleistocene–Holocene volcanic activity of La Palma using the unspiked K–Ar technique. J. Volcanol. Geotherm. Res. 86, 137–149. https://doi.org/10.1016/S0377-0273(98)00074-2.
Guillou, H., Carracedo, J.C., Duncan, R.A., 2001. K–Ar, 40Ar–39Ar ages and magnetostratigraphy of Brunhes and Matuyama lava sequences from La Palma Island. J. Volcanol. Geotherm. Res. 106, 175–194. https://doi.org/10.1016/S0377-0273(00)00294-8.
Gurenko, A.A., Hoernle, K.A., Hauff, F., Schmincke, H.-U., Han, D., Miura, Y.N., Kaneoka, I., 2006. Major, trace element and Nd–Sr–Pb–O–He–Ar isotope signatures of shield stage lavas from the central and western Canary Islands: insights into mantle and crustal processes. Chem. Geol. 233, 75–112. https://doi.org/10.1016/j.chemgeo.2006.02.016.
Gurenko, A.A., Sobolev, A.V., Hoernle, K.A., Hauff, F., Schmincke, H.-U., 2009. Enriched, HIMU-type peridotite and depleted recycled pyroxenite in the Canary plume: a mixed-up mantle. Earth Planet. Sci. Lett. 277, 514–524. https://doi.org/10.1016/j.epsl.2008.11.013.
Halldórsson, S.A., Hilton, D.R., Scarsi, P., Abebe, T., Hopp, J., 2014. A common mantle plume source beneath the entire East African rift system revealed by coupled helium-neon systematics: helium-neon isotopes in the ears. Geophys. Res. Lett. 41, 2304–2311. https://doi.org/10.1002/2014GL059424.
Hansteen, T.H., Klugel, A., 2008. Fluid inclusion thermobarometry as a tracer for magmatic processes. Rev. Mineral. Geochem. 69, 143–177. https://doi.org/10.2138/rmg.2008.69.5.
Hilton, D.R., Hammerschmidt, K., Teufel, S., Friedrichsen, H., 1993. Helium isotope characteristics of Andean geothermal fluids and lavas. Earth Planet. Sci. Lett. 120, 265–282. https://doi.org/10.1016/0012-821X(93)90244-4.
Hilton, D.R., Barling, J., Wheller, G.E., 1995. Effect of shallow-level contamination on the helium isotope systematics of ocean-island lavas. Nature 373, 330–333. https://doi.org/10.1038/373330a0.
Hilton, D.R., Macpherson, C.G., Elliott, T.R., 2000. Helium isotope ratios in mafic phenocrysts and geothermal fluids from La Palma, the Canary Islands (Spain): implications for HIMU mantle sources. Geochim. Cosmochim. Acta 64, 2119–2132. https://doi.org/10.1016/S0016-7037(00)00358-6.
Hoernle, K., Tilton, G., Schmincke, H.-U., 1991. SrNdPb isotopic evolution of Gran Canaria: evidence for shallow enriched mantle beneath the Canary Islands. Earth Planet. Sci. Lett. 106, 44–63. https://doi.org/10.1016/0012-821X(91)90062-M.
Hoernle, K., Zhang, Y.-S., Graham, D., 1995. Seismic and geochemical evidence for large-scale mantle upwelling beneath the eastern Atlantic and western and Central Europe. Nature 374, 34–39. https://doi.org/10.1038/374034a0.
Holik, J.S., Rabinowitz, P.D., Austin, J.A., 1991. Effects of Canary hotspot volcanism on structure of oceanic crust off Morocco. J. Geophys. Res. 96, 12039. https://doi.org/10.1029/91JB00709.
Hopp, J., Trieloff, M., Altherr, R., 2004. Neon isotopes in mantle rocks from the Red Sea region reveal large-scale plume–lithosphere interaction. Earth Planet. Sci. Lett. 219, 61–76. https://doi.org/10.1016/S0012-821X(03)00691-5.
Hopp, J., Trieloff, M., Altherr, R., 2007. Noble gas compositions of the lithospheric mantle below the Chyulu Hills volcanic field, Kenya. Earth Planet. Sci. Lett. 261, 635–648. https://doi.org/10.1016/j.epsl.2007.07.027.
Jackson, M.D., Blundy, J., Sparks, R.S.J., 2018. Chemical differentiation, cold storage and remobilization of magma in the Earth's crust. Nature 564, 405–409. https://doi.org/10.1038/s41586-018-0746-2.
Jiménez-Mejías, M., Andújar, J., Scaillet, B., Casillas, R., 2022. Experimental determination of H 2 O and CO 2 solubilities of mafic alkaline magmas from Canary Islands. C. R. Géosci. 353, 289–314. https://doi.org/10.5802/crgeos.84.
Keppler, H., Cialdella, L., Couffignal, F., Wiedenbeck, M., 2022. The solubility of N2 in silicate melts and nitrogen partitioning between upper mantle minerals and basalt. Contrib. Mineral. Petrol. 177, 83. https://doi.org/10.1007/s00410-022-01948-z.
Klügel, A., Hansteen, T.H., Galipp, K., 2005. Magma storage and underplating beneath Cumbre Vieja volcano, La Palma (Canary Islands). Earth Planet. Sci. Lett. 236, 211–226. https://doi.org/10.1016/j.epsl.2005.04.006.
Klügel, A., Longpré, M.-A., García-Cañada, L., Stix, J., 2015. Deep intrusions, lateral magma transport and related uplift at ocean island volcanoes. Earth Planet. Sci. Lett. 431, 140–149. https://doi.org/10.1016/j.epsl.2015.09.031.
Klügel, A., Galipp, K., Hoernle, K., Hauff, F., Groom, S., 2017. Geochemical and volcanological evolution of La Palma, Canary Islands. J. Petrol. 58, 1227–1248. https://doi.org/10.1093/petrology/egx052.
Lages, J., Rizzo, A.L., Aiuppa, A., Samaniego, P., Le Pennec, J.L., Ceballos, J.A., Narváez, P.A., Moussallam, Y., Bani, P., Schipper, C.I., Hidalgo, S., Gaglio, V., Alberti, E., Sandoval-Velasquez, A., 2021. Noble gas magmatic signature of the Andean Northern Volcanic Zone from fluid inclusions in minerals. Chem. Geol. 559, 119966 https://doi.org/10.1016/j.chemgeo.2020.119966.
Lee, J.-Y., Marti, K., Severinghaus, J.P., Kawamura, K., Yoo, H.-S., Lee, J.B., Kim, J.S., 2006. A redetermination of the isotopic abundances of atmospheric Ar. Geochim. Cosmochim. Acta 70, 4507–4512. https://doi.org/10.1016/j.gca.2006.06.1563.
Libourel, G., Marty, B., Humbert, F., 2003. Nitrogen solubility in basaltic melt. Part I. Effect of oxygen fugacity. Geochim. Cosmochim. Acta 67, 4123–4135. https://doi.org/10.1016/S0016-7037(03)00259-X.
Longpré, M.-A., 2021. Reactivation of Cumbre Vieja volcano. Science 374, 1197–1198. https://doi.org/10.1126/science.abm9423.
Longpré, M.-A., Felpeto, A., 2021. Historical volcanism in the Canary Islands; part 1: a review of precursory and eruptive activity, eruption parameter estimates, and implications for hazard assessment. J. Volcanol. Geotherm. Res. 419, 107363 https://doi.org/10.1016/j.jvolgeores.2021.107363.
Lupton, J.E., Arculus, R.J., Evans, L.J., Graham, D.W., 2012. Mantle hotspot neon in basalts from the Northwest Lau Back-arc Basin: hotspot neon in the NW Lau back-arc Bsain. Geophys. Res. Lett. 39 https://doi.org/10.1029/2012GL051201 n/a-n/a.
Madureira, P., Moreira, M., Mata, J., Allegre, C., 2005. Primitive neon isotopes in Terceira Island (Azores archipelago). Earth Planet. Sci. Lett. 233, 429–440. https://doi.org/10.1016/j.epsl.2005.02.030.
Marcantonio, F., Zindler, A., Elliott, T., Staudigel, H., 1995. Os isotope systematics of La Palma, Canary Islands: evidence for recycled crust in the mantle source of HIMU Ocean islands. Earth Planet. Sci. Lett. 133, 397–410. https://doi.org/10.1016/0012-821X(95)00092-Q.
Martinez-Arevalo, C., de Mancilla, F.L., Helffrich, G., Garcia, A., 2013. Seismic evidence of a regional sublithospheric low velocity layer beneath the Canary Islands. Tectonophysics 608, 586–599. https://doi.org/10.1016/j.tecto.2013.08.021.
Moreira, M., Kunz, J., Allègre, C., 1998. Rare gas systematics in popping rock: isotopic and elemental compositions in the upper mantle. Science 279, 1178–1181. https://doi.org/10.1126/science.279.5354.1178.
Moreira, M., Doucelance, R., Kurz, M.D., Dupré, B., Allègre, C.J., 1999. Helium and lead isotope geochemistry of the Azores Archipelago. Earth Planet. Sci. Lett. 169, 189–205. https://doi.org/10.1016/S0012-821X(99)00071-0.
Mundl-Petermeier, A., Walker, R.J., Fischer, R.A., Lekic, V., Jackson, M.G., Kurz, M.D., 2020. Anomalous 182W in high 3He/4He ocean island basalts: fingerprints of Earth's core? Geochim. Cosmochim. Acta 271, 194–211. https://doi.org/10.1016/j.gca.2019.12.020.
Mundl-Petermeier, A., Viehmann, S., Tusch, J., Bau, M., Kurzweil, F., Münker, C., 2022. Earth's geodynamic evolution constrained by 182W in Archean seawater. Nat. Commun. 13, 2701. https://doi.org/10.1038/s41467-022-30423-3.
Ntaflos, T., Casetta, F., Sandoval-Velasquez, A., Rizzo, A.L., Aiuppa, A., Alonso, M., Padron, E., Pankhurst, M., Perez, N., 2022. Mantle-Derived Xenoliths from the Cumbre Vieja 2021 Lava Flows: Insights on the Composition of the Lithosphere Beneath La Palma (Canary Islands) (Other). Display. https://doi.org/10.5194/egusphere-egu22-12452.
Nuccio, P.M., Paonita, A., Rizzo, A., Rosciglione, A., 2008. Elemental and isotope covariation of noble gases in mineral phases from Etnean volcanics erupted during 2001–2005, and genetic relation with peripheral gas discharges. Earth Planet. Sci. Lett. 272, 683–690. https://doi.org/10.1016/j.epsl.2008.06.007.
Ozima, M., Podosek, F.A., 2002. Noble Gas Geochemistry. Cambridge University Press.
Padrón, E., Pérez, N.M., Hernández, P.A., Sumino, H., Melián, G.V., Barrancos, J., Nolasco, D., Padilla, G., Dionis, S., Rodríguez, F., Hernández, Í., Calvo, D., Peraza, M. D., Nagao, K., 2013. Diffusive helium emissions as a precursory sign of volcanic unrest. Geology 41, 539–542. https://doi.org/10.1130/G34027.1.
Padrón, E., Pérez, N.M., Rodríguez, F., Melián, G., Hernández, P.A., Sumino, H., Padilla, G., Barrancos, J., Dionis, S., Notsu, K., Calvo, D., 2015. Dynamics of diffuse carbon dioxide emissions from Cumbre Vieja volcano, La Palma, Canary Islands. Bull. Volcanol. 77, 28. https://doi.org/10.1007/s00445-015-0914-2.
Padrón, E., Pérez, N.M., Hernández, P.A., Sumino, H., Melián, G.V., Alonso, M., Rodríguez, F., Asensio-Ramos, M., D'Auria, L., 2022. Early precursory changes in the ^{3} He/ ^{4} He ratio prior to the 2021 Tajogaite eruption at Cumbre Vieja volcano, La Palma, Canary Islands. Geophys. Res. Lett. 49 https://doi.org/10.1029/2022GL099992.
Pankhurst, M.J., Scarrow, J.H., Barbee, O.A., Hickey, J., Coldwell, B.C., Rollinson, G.K., Rodríguez-Losada, J.A., Martín Lorenzo, A., Rodríguez, F., Hernández, W., Calvo

Fernández, D., Hernández, P., Pérez, N.M., 2022. Rapid response petrology for the opening eruptive phase of the 2021 Cumbre Vieja eruption, La Palma, Canary Islands. Volcanica 5, 1–10. https://doi.org/10.30909/vol.05.01.0110.

Papale, P., Moretti, R., Paonita, A., 2022. Thermodynamics of multi-component gas–melt equilibrium in magmas: theory, models, and applications. Rev. Mineral. Geochem. 87, 431–556. https://doi.org/10.2138/rmg.2022.87.10.

Parley, K.A., Craig, H., 1994. Atmospheric argon contamination of ocean island basalt olivine phenocrysts. Geochim. Cosmochim. Acta 58, 2509–2517. https://doi.org/10.1016/0016-7037(94)90027-2.

Pérez, N.M., Nakai, S., Wakita, H., Sano, Y., Williams, S.N., 1994. 3He/4He isotopic ratios in volcanic-hydrothermal discharges from the Canary Islands, Spain: implications on the origin of the volcanic activity. Mineral. Mag. 58, 709–710. https://doi.org/10.1180/minmag.1994.58A.2.107.

Peters, B.J., Mundl-Petermeier, A., Horan, M.F., Carlson, R.W., Walker, R.J., 2019. Chemical separation of tungsten and other trace elements for TIMS isotope ratio measurements using organic acids. Geostand. Geoanal. Res. 43, 245–259. https://doi.org/10.1111/ggr.12259.

Pouchou, J.-L., Pichoir, F., 1991. Quantitative analysis of homogeneous or stratified microvolumes applying the model "PAP". In: Heinrich, K.F.J., Newbury, D.E. (Eds.), Electron Probe Quantitation. Springer US, Boston, MA, pp. 31–75. https://doi.org/10.1007/978-1-4899-2617-3_4.

Rizzo, A.L., Barberi, F., Carapezza, M.L., Di Piazza, A., Francalanci, L., Sortino, F., D'Alessandro, W., 2015. New mafic magma refilling a quiescent volcano: evidence from He-Ne-Ar isotopes during the 2011-2012 unrest at Santorini, Greece: research article. Geochem. Geophys. Geosyst. 16, 798–814. https://doi.org/10.1002/2014GC005653.

Rizzo, A.L., Faccini, B., Casetta, F., Faccincani, L., Ntaflos, T., Italiano, F., Coltorti, M., 2021. Melting and metasomatism in West Eifel and Siebengebirge sub-continental lithospheric mantle: evidence from concentrations of volatiles in fluid inclusions and petrology of ultramafic xenoliths. Chem. Geol. 581, 120400 https://doi.org/10.1016/j.chemgeo.2021.120400.

Sandoval Velasquez, A., Rizzo, A.L., Aiuppa, A., Coltorti, M., 2022b. The radiogenic nature of the lithospheric mantle beneath Lanzarote (Canary Islands). In: Presented at the Congresso SGI-SIMP, Società Geologica Italiana. https://doi.org/10.3301/ABSGI.2022.02.

Sandoval Velasquez, A., Rizzo, A.L., Casetta, F., Ntaflos, T., Aiuppa, A., Alonso, M., Padrón, E., Pankhurst, M., Perez, N.M., 2022c. The nature of the lithospheric mantle under La Palma (Canary Islands): new data on noble gases and CO2 isotopes from the 2021 Cumbre Vieja eruption. In: Conferenza A. Rittmann.

Sandoval-Velasquez, A., Rizzo, A.L., Aiuppa, A., Remigi, S., Padrón, E., Pérez, N.M., Frezzotti, M.L., 2021. Recycled crustal carbon in the depleted mantle source of El Hierro volcano, Canary Islands. Lithos 400–401, 106414. https://doi.org/10.1016/j.lithos.2021.106414.

Sano, Y., Kagoshima, T., Takahata, N., Nishio, Y., Roulleau, E., Pinti, D.L., Fischer, T.P., 2015. Ten-year helium anomaly prior to the 2014 Mt Ontake eruption. Sci. Rep. 5, 13069. https://doi.org/10.1038/srep13069.

Schmincke, H.-U., 1982. Volcanic and chemical evolution of the Canary Islands. In: von Rad, U., Hinz, K., Sarnthein, M., Seibold, E. (Eds.), Geology of the Northwest African Continental Margin. Springer Berlin Heidelberg, Berlin, Heidelberg, pp. 273–306. https://doi.org/10.1007/978-3-642-68409-8_12.

Schneider, C.A., Rasband, W.S., Eliceiri, K.W., 2012. NIH Image to ImageJ: 25 years of image analysis. Nat. Methods 9, 671–675. https://doi.org/10.1038/nmeth.2089.

Span, R., Wagner, W., 1996. A new equation of state for carbon dioxide covering the fluid region from the triple-point temperature to 1100 K at pressures up to 800 MPa. J. Phys. Chem. Ref. Data Monogr. 25, 1509–1596. https://doi.org/10.1063/1.555991.

Sterner, S.M., Bodnar, R.J., 1984. Synthetic fluid inclusions in natural quartz I. Compositional types synthesized and applications to experimental geochemistry. Geochim. Cosmochim. Acta 48, 2659–2668. https://doi.org/10.1016/0016-7037(84)90314-4.

Sterner, S.M., Bodnar, R.J., 1991. Synthetic fluid inclusions; X, experimental determination of P-V-T-X properties in the CO 2 -H 2 O system to 6 kb and 700 degrees C. Am. J. Sci. 291, 1–54. https://doi.org/10.2475/ajs.291.1.1.

Thiery, R., Vidal, J., Dubessy, J., 1994. Phase equilibria modelling applied to fluid inclusions: liquid-vapour equilibria and calculation of the molar volume in the CO2 CH4 N2 system. Geochim. Cosmochim. Acta 58, 1073–1082. https://doi.org/10.1016/0016-7037(94)90573-8.

Torgersen, T., Jenkins, W.J., 1982. Helium isotopes in geothermal systems: Iceland, the Geysers, Raft River and Steamboat Springs. Geochim. Cosmochim. Acta 46, 739–748. https://doi.org/10.1016/0016-7037(82)90025-4.

Torres-González, P.A., Luengo-Oroz, N., Lamolda, H., D'Alessandro, W., Albert, H., Iribarren, I., Moure-García, D., Soler, V., 2020. Unrest signals after 46 years of quiescence at Cumbre Vieja, La Palma, Canary Islands. J. Volcanol. Geotherm. Res. 392, 106757 https://doi.org/10.1016/j.jvolgeores.2019.106757.

Troll, V.R., Carracedo, J.C., 2016. The Geology of the Canary Islands. Elsevier. https://doi.org/10.1016/C2015-0-04268-X.

Vance, D., Stone, J.O.H., O'Nions, R.K., 1989. He, Sr and Nd isotopes in xenoliths from Hawaii and other oceanic islands. Earth Planet. Sci. Lett. 96, 147–160. https://doi.org/10.1016/0012-821X(89)90129-5.

Zanon, V., Pimentel, A., Auxerre, M., Marchini, G., Stuart, F.M., 2020. Unravelling the magma feeding system of a young basaltic oceanic volcano. Lithos 352–353, 105325. https://doi.org/10.1016/j.lithos.2019.105325.

Zindler, A., Hart, S., 1986. Chemical geodynamics. Annu. Rev. Earth Planet. Sci. 14, 493–571. https://doi.org/10.1146/annurev.ea.14.050186.002425.